

Chaotic Control Theory Applied to the Chirikov Standard Map

PHYC40260: Projects in Theoretical Physics

Conor Finn - 08644209

Abstract

The aim of the first part of this project was to gain an understanding and appreciation of the complex dynamics that arise from the apparent simplicity of the single parameter Chirikov standard map. We examined how, and where, the standard map can appear, in particular, how the dynamics of the standard map are the same as the underlying dynamics of the bouncing ball problem. We examined the important features of the the dynamics of the standard map, in particular, at the dynamics near fixed points of the map. We looked at how the complicated winding upon winding of the stable and unstable manifolds near hyperbolic fixed points leads to the existence of Smale horseshoes, and how this induces the complicated chaotic dynamics in the regions near hyperbolic fixed points. We then moved on to consider elliptic fixed points and the complicated “microcosms within microcosms” around these fixed points, but how this complexity is kept well behaved by the existence of KAM curves. This naturally led us on to KAM theory, the theory that describes the break-up of KAM curves. We considered some of the most important, and relevant results from KAM theory.

The aim of the second part of this project was to apply chaotic control theory to a system that has, or is very close to having, the dynamics of the Chirikov standard map. We applied the linear quadric regulator (LQR) control design method, to the aforementioned bouncing ball problem, and examined how this method not only allow us to control the bouncing ball, but provides optimal.

The first part is largely based on / follows [1] and takes elements from [7], while the second part is based on [8] and [9]. The original work includes writing MATLAB scripts/codes to create images to supplement the report. We also examined the sensitivity of the control method to non-optimal control, validating the LQR control design method as a method for obtain optimal control.

Contents

I The Chirikov Standard Map	3	III Appendices	36
1 Derivations	3	9 Area-Preserving Twist Maps	36
1.1 High Bounce Map	3	10 Discrete Time LQR	36
1.2 The Microtron Accelerator	4	11 MATLAB Scripts	38
2 The Chirikov Standard Map	6	11.1 M-Files for Fig. 2.1 and figs. 2.2	38
2.1 Informal Introduction	6	11.2 M-Files for Figs. 2.3	39
2.2 Formal Introduction	6	11.2.1 M-File for Fig. 2.3 (a)	39
3 Near-Integrable Systems	10	11.2.2 M-File for Fig. 2.3 (b)	39
3.1 Rotation Number	10	11.2.3 M-File for Fig. 2.3 (c)	40
3.2 Fixed Points	10	11.3 M-File for Fig. 3.1	40
3.3 Linearisation	12	11.4 M-File for Fig. 3.1	41
4 Hyperbolic Fixed Points	14	11.5 M-File for Figs. 4.6	42
4.1 Invariant Curves	14	11.6 M-File for Figs. 5.5	43
4.2 Invariant Curves in the Standard Map	16	11.7 M-Files for Sec. 8.6	44
4.2.1 (First order) Equilibrium points of our Map	16	11.7.1 M-File for Linearisation	44
4.2.2 Calculating the Jacobian for each Fixed Point	17	11.7.2 M-File for Figs. 8.1	45
4.2.3 Classification of fixed points .	17		
4.2.4 The Unstable Manifold . . .	17		
4.3 StdMap	17		
5 Elliptic Fixed Points	24		
5.1 Microcosms within Microcosms . .	24		
5.2 Numerical Example	25		
6 KAM Theory	28		
6.1 The Importance of KAM Curves . .	28		
6.2 Moser's Twist Theorem	28		
6.3 The Break-up of KAM Curves . .	29		
II Chaotic Control	31		
7 Chaotic Control Theory	31		
7.1 Why are we interested?	31		
7.2 What is Chaotic Control?	31		
8 Controlling a Bouncing Ball	31		
8.1 High Ball Map under Frequency Control	31		
8.2 Optimal Control	32		
8.3 Fixed Points	32		
8.4 Linearisation	32		
8.5 LQR Method	33		
8.6 Ball under Control	34		

Part I. The Chirikov Standard Map

1 Derivations

1.1 High Bounce Map

The bouncing ball system is a simple system which yields the standard map. It consists of a ball bouncing on sinusoidally oscillating surface / plate. The oscillation of the plate drives the system. The vertical displacement of the plate x at a time t is given by

$$x(t) = A \sin(\omega t + \theta) \quad (1.1)$$

where A , ω and θ are the amplitude, the frequency and the phase angle of the plate's oscillation, respectively. The ball bounces on this plate, and the vertical displacement of the ball at a particular time is given by $y(t)$. Between each bounce there is a certain flight time τ . In the most general case, this flight time is not the same for each bounce.

Each bounce is a discrete event: this allows us to reduce this continuous system to a discrete map. The time of flight of the ball preceding the k -th bounce is then given by $\tau_k = t_k - t_{k-1}$ where t_k is the time at which the k -th bounce occurs and t_{k-1} is the time at which the prior bounce occurred. At time t_{k+1} the plate's vertical position is

$$\begin{aligned} x_{k+1} &= A \sin(\omega \tau_{k+1} + \theta_k) \\ &= A \sin(\omega(t_{j+1} - t_j) + \theta_k) \end{aligned} \quad (1.2)$$

where θ_k is the phase angle of the plate at the time of the prior bounce, i.e.

$$\theta_k = \omega \tau_k + \theta_{k-1} \quad (1.3)$$

It then follows that at the next bounce

$$\theta_{k+1} = \omega \tau_{k+1} + \theta_k \quad (1.4)$$

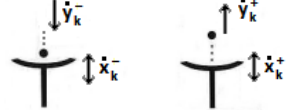
Which allows us to rewrite eqn. 1.2 as

$$x_{k+1} = A \sin(\theta_{k+1}) \quad (1.5)$$

Thus, the velocity of the plate at time t_{k+1} is given by

$$\begin{aligned} \frac{d}{dt} \{x_{k+1}\} &= \frac{d}{dt} \{A \sin(\omega(t_{j+1} - t_j) + \theta_k)\} \\ \dot{x}_{k+1} &= A \omega \cos(\omega(t_{j+1} - t_j) + \theta_k) \\ &= A \omega \cos(\omega \tau_{k+1} + \theta_k) \\ &= A \omega \cos(\theta_{k+1}) \end{aligned} \quad (1.6)$$

Fig. 1.1 – Pre-bounce and post-bounce velocities.



Now, at the time t_{k+1} a collision between the ball and the plate will occur, and we have not yet taken this into account, so we will introduce the following notation: the superscript “−” and “+” on a particular quantity denotes whether we are considering the quantity just before or just after the bounce, respectively. Having introduced this notation eqn. 1.6 becomes

$$\dot{x}_{k+1}^- = A \omega \cos(\theta_{k+1}) \quad (1.7)$$

We will now consider the effect of the impact on the system. Conservation of momentum gives

$$\begin{aligned} m_p \dot{x}_k^- + m_b \dot{y}_k^- &= m_p \dot{x}_k^+ + m_b \dot{y}_k^+ \\ \iff \dot{x}_k^- + M \dot{y}_k^- &= \dot{x}_k^+ + M \dot{y}_k^+ \end{aligned} \quad (1.8)$$

where \dot{y}_k^\pm is the velocity of the ball before/after the k -th bounce, m_p and m_b are the masses of the plate and the ball, respectively, while $M \equiv m_b/m_p$ is the ratio of the mass of the ball to the mass of the plate. If the ratio of the relative velocities of the ball and the plate before and after a bounce is e , the coefficient of restitution, then

$$\dot{y}_k^+ - \dot{x}_k^+ = -e (\dot{y}_k^- - \dot{x}_k^-) \quad (1.9)$$

where the negative sign is a consequence of the reversal of directions of relative velocities. Now, rearranging eqn. 1.8 and inserting into eqn. 1.9 to eliminate \dot{x}_k^+ gives us

$$\dot{y}_k^+ = a_1 \dot{x}_k^- + a_2 \dot{y}_k^- \quad (1.10)$$

where

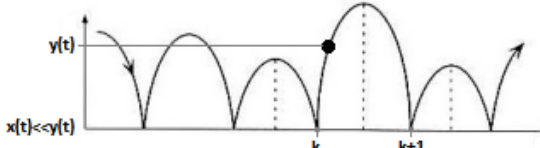
$$a_1 \equiv \left(\frac{1+e}{1+M} \right) \quad \text{and} \quad a_2 \equiv \left(\frac{M-e}{1+M} \right)$$

Evaluating at the time of the next bounce instead of the current bounce yields

$$\dot{y}_{k+1}^+ = a_1 \dot{x}_{k+1}^- + a_2 \dot{y}_{k+1}^- \quad (1.11)$$

We will now introduce the *high bounce approximation* which is the assumption that the maximum

Fig. 1.2 – The high bounce approximation: the amplitude of the oscillations of the plate are small compared to the height of each bounce so it can be assumed that each flight is approximately symmetrical, thus, ascent speed is approximately the same as descent speed.



height attained by the ball during its flight between each bounce is much larger than the amplitude of the oscillations of the plate, i.e. $y_{max} \gg x_{max} = A$. As such, the height the ball descends is approximately the same as the height the ball ascends, thus the magnitude of the velocity on ascent is the same as the magnitude velocity on descent, i.e.

$$\dot{y}_{k+1}^- = -\dot{y}_k^+ \quad (1.12)$$

It also gives us that the time of flight before the $(k+1)$ -th bounce is given by

$$\tau_{k+1} = \frac{2\dot{y}_k^+}{g} \quad (1.13)$$

where g is the acceleration due to gravity. It follows from these two equations along with eqn. 1.7 that eqns. 1.4 and 1.11 may be written as

$$\dot{y}_{k+1}^+ = -a_2 \dot{y}_k^+ + a_1 A \omega \cos(\theta_{k+1}) \quad (1.14a)$$

$$\theta_{k+1} = \theta_k + \omega \left(\frac{2\dot{y}_k^+}{g} \right) \mod 2\pi \quad (1.14b)$$

This is the *high bounce map*¹. The dynamics of this map are closely related to the dynamics of the standard map: in fact, with two further assumptions we get the exact standard map. We shall now show that this is indeed the case.

We make two further assumptions: firstly, that the plate has a large mass relative to the ball and so is practically unperturbed by the impact with

¹ When eqns. 8.1 are iterated to produce a dynamical solution, eqn. 1.14b is evaluated *modulo* 2π since the θ refers to a physical position of the plate. Eqn. 1.14a is not evaluated *modulo* 2π since the plate may go through more than one cycle before the next bounce. Thus, we see that the cylindrical representation (eqns. 2.3) is the natural representation for the high bounce map. More about this in sec. 2.2.

the ball ($M = m_b/m_p \approx 0$); secondly, that the collisions are perfectly elastic ($e = 1$). Under these assumptions, $a_1 = 2$ and $a_2 = -1$. Hence, we now have

$$\dot{y}_{k+1}^+ = \dot{y}_k^+ + 2\omega A \cos(\theta_{k+1}) \quad (1.15a)$$

$$\theta_{k+1} = \theta_k + \omega \left(\frac{2\dot{y}_k^+}{g} \right) \mod 2\pi \quad (1.15b)$$

Which is the standard map, although it is not yet apparently obvious. To see this explicitly, multiply eqn. 1.15a through by $2\omega/g$ yielding

$$\begin{aligned} \frac{2\omega}{g} \dot{y}_{k+1}^+ &= \frac{2\omega}{g} \dot{y}_k^+ + \frac{4\omega^2}{g} A \cos(\theta_{k+1}) \\ \theta_{k+1} &= \theta_k + \left(\frac{2\omega}{g} \right) \dot{y}_k^+ \mod 2\pi \end{aligned}$$

We perform a rescaling by setting

$$r_k \equiv \frac{2\omega}{g} \dot{y}_k^+ \quad \text{and} \quad K \equiv \frac{4\omega^2}{g} A$$

and we also perform a shift of the phase by $-\pi/2$ yielding

$$\begin{aligned} r_{k+1} &= r_k + K \sin(\theta_{k+1}) \\ \theta_{k+1} &= \theta_k + r_k \mod 2\pi \end{aligned}$$

which is the standard map.

1.2 The Microtron Accelerator

For a more physically interesting situation where one might encounter the standard map we turn to the relativistic motion of an electron in a microtron accelerator, see fig. 1.3.

A relativistic electron passes through a gap: in this gap there is a (spatially) uniform time-dependent electric field given by

$$\varepsilon = \varepsilon_0 \sin(\omega t) \quad (1.18)$$

This electric field acts to accelerate or decelerate the electron, this results in a change of kinetic energy

$$\Delta E_n = e\varepsilon_0 d \sin(\omega t_n) \quad (1.19)$$

where t_n is the time at which the electron passes through the gap. Since the electron is relativistic, it is assumed that the time it takes to traverse the gap is negligible, and so the change electric field during this time is also negligible.

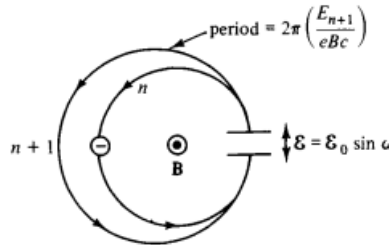


Fig. 1.3 – The Microtron Accelerator. Image taken from [1].

Outside the gap the electron orbits around due to a uniform magnetic field B . The period of this orbit is

$$T = 2\pi \left(\frac{mc}{eB} \right) = 2\pi \left(\frac{E}{eBc} \right) \quad (1.20)$$

where E is the electron's relativistic energy (where we are neglecting losses due to synchrotron radiation). Now,

$$\begin{aligned} E_{n+1} &= E_n + \Delta E_n \\ &= E_n + K \sin(\theta_n) \end{aligned}$$

where $K \equiv e\varepsilon_0 d$, and E_n is the energy of the electron prior to the n -th passing of the electron through the gap, and finally, θ_n is the phase of the electric field at that time, i.e. $\theta_n = \omega t_n$. However, we also have that the phase at the $(n+1)$ -th transition is given by

$$\theta_{n+1} = \theta_n + \beta E_{n+1} \quad (1.21a)$$

where $\beta \equiv 2\pi\omega/eBc$. However, we can see again that these two equations constitute the standard map.

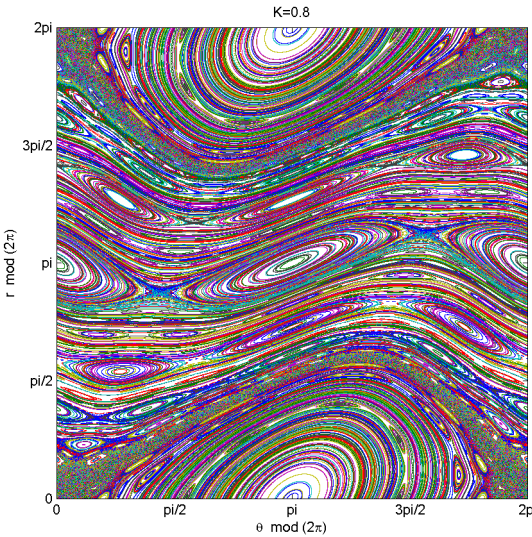


Fig. 2.1 – The standard map for $K = 0.8$. Here, we have taken 1,000 different initial conditions, randomly distributed throughout the phase space, and iterated them through the standard map (eqns. 2.1) 5,000 times. We have represented different initial conditions with different colours to help differentiate between each set of iterations. See sec. 11.1 for the MATLAB script used to create this plot.

2 The Chirikov Standard Map

2.1 Informal Introduction

Before we make examine any of the formal theory surrounding the standard map, it is perhaps best if we got a “feel” for it. The best way of doing this is to simply preform iterations of the map for various initial conditions. We will preform the iterations of the map in it’s toroidal representation (see sec. 2.2 for more details about the various representations). The standard map in it’s toroidal representation is

$$r_{n+1} = r_n + K \sin(\theta_n) \mod 2\pi \quad (2.1a)$$

$$\theta_{n+1} = \theta_n + r_{n+1} \mod 2\pi \quad (2.1b)$$

Now, we will simply pick a value for K and many different initial conditions and iterate them through the map many times. Fig. 2.1 shows us the standard map for $K = 0.8$: from this we can see that the standard map leads to a rich set of dynamics.

However, this is only one possible choice for the value of K : figs. 2.2 shows us the standard map for various increasing values of K . We can see that the standard map seems to be completely regular

for $K = 0$ but that chaotic regions grow and eventually start to dominate the phase space for higher values of K . This is not surprising: K represents how hard we are driving our system as it is the parameter that defines how small, or large, the periodic kicking of our system is, so we would not expect any chaotic behaviour if we are not perturbing the system in any way. The goal of part I is to first gain and understanding of the dynamics for a particular value of K before culminating in sec. 6 which introduces KAM theory: this theory shows us how the chaos spreads from small regions of the phase space for small values of K to dominating the phase space for higher values of K .

2.2 Formal Introduction

The standard map was proposed by Boris Chirikov as a paradigm for resonance phenomena in conservative systems, it was also derived independently by Bryan Taylor as a model for the motion of charge particles in a strong magnetic field (hence it is sometimes referred to as the Chirikov–Taylor map). It is an area-preserving map for two dynamical variables: in fact, it is one of a particular class of maps called “area-preserving twist maps” (see sec. 9). The standard map also has many symmetries, most important of which is the time-reversibility symmetry (given an iterate we can calculate the prior iterate with an inverse).

The following is one of the many canonical forms of the map

$$r_{n+1} = r_n + K \sin(\theta_n) \quad (2.2a)$$

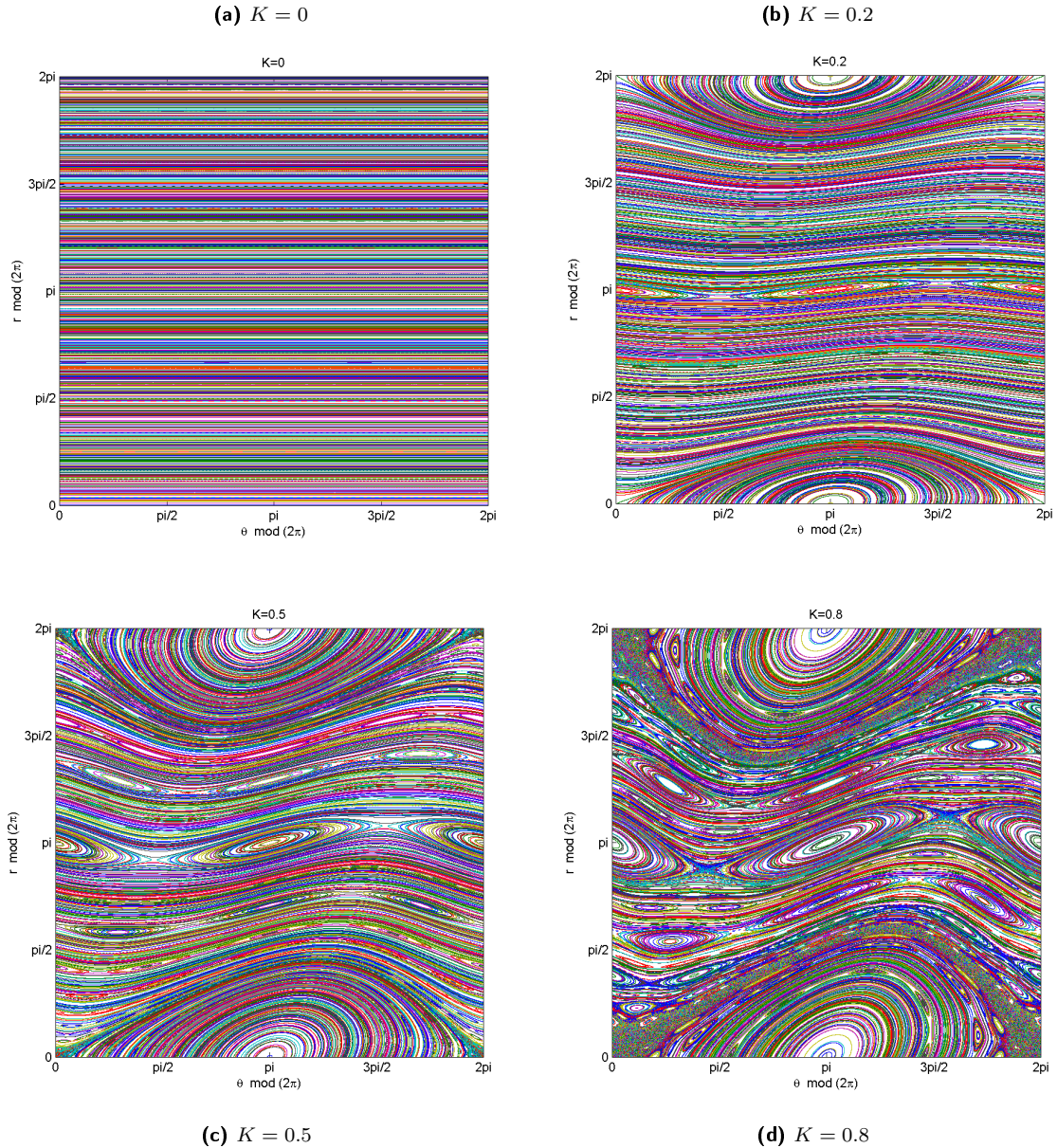
$$\theta_{n+1} = \theta_n + r_{n+1} \quad (2.2b)$$

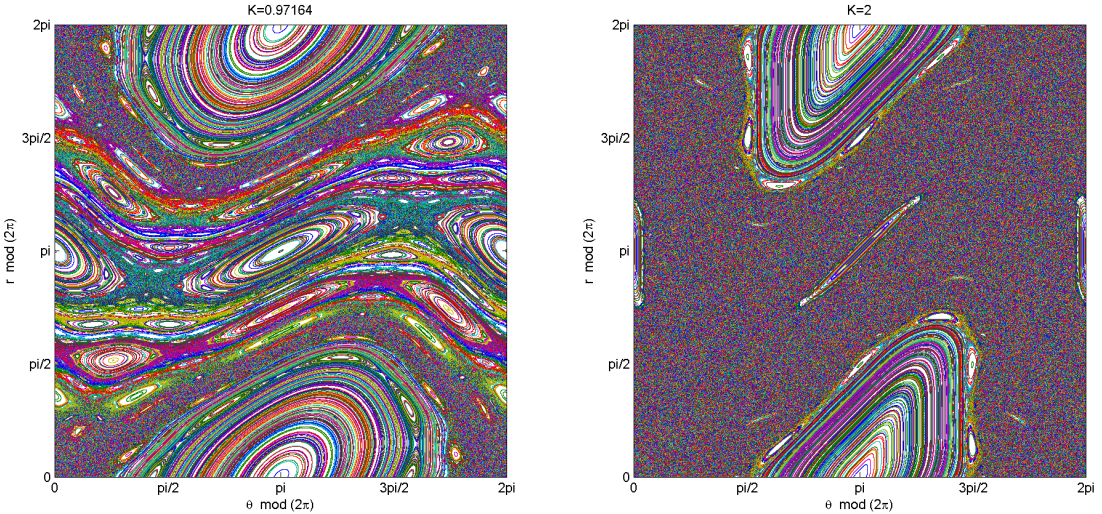
This may be seen, perhaps, most naturally in polar coordinates where the value of r becomes the magnitude of the radial vector and θ is, of course, the polar angle. In the language of topology, this representation is in $\mathbb{R}_+ \times S^1$ ($r \in \mathbb{R}_+, \theta \in S^1$).

However, depending on the nature of the system from which the map was derived, it might be more useful to represent the map in different spaces. For example, if the system from which eqns. 2.2 was derived allowed the r values to be negative, then the polar representation would be inappropriate.

Then, one might perhaps chose a cylindrical space $\mathbb{R}^1 \times S^1$ ($r \in \mathbb{R}, \theta \in S^1$) in which θ and $\theta + 2\pi$ are considered to be the exact same point, or put another way

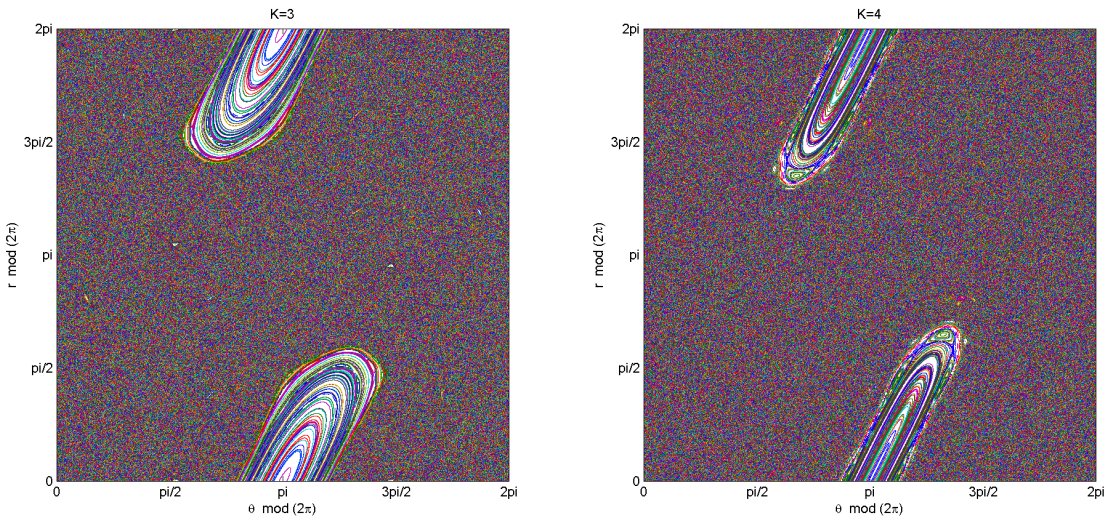
Fig. 2.2 – The standard map for various values of K . Note in particular the growing chaotic region as K increases. See sec. 11.1 for the MATLAB script used to create this plot.





(e) $K = 0.97164$. We shall see at the end of part I why we have take such a particular value for K .

(f) $K = 2$



(g) $K = 3$

(h) $K = 4$

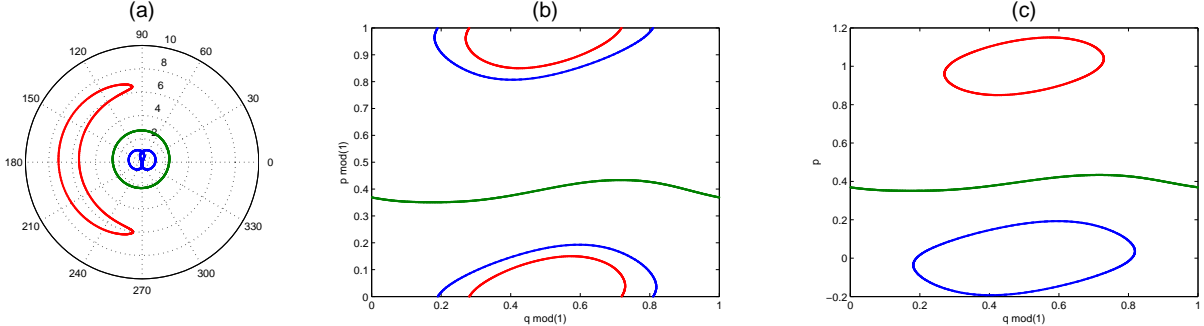


Fig. 2.3 – Various representations for $K = 0.5$: (a) Polar map $\mathbb{R}_+ \times S^1$; (b) Two-Torus map $T^2 = S^1 \times S^1$; (c) Cylindrical map $\mathbb{R}^1 \times S^1$. It should be noted that each of the 3 separate colours corresponds to a different initial starting point for our iterations and that the same colour represents the same initial conditions for each separate representation. Each initial condition has been iterated 1000 times. See sec. 11.2 for the MATLAB scripts used to create these plots.

$$r_{n+1} = r_n + K \sin(\theta_n) \quad (2.3a)$$

$$\theta_{n+1} = \theta_n + r_{n+1} \bmod 2\pi \quad (2.3b)$$

As before, one must pay heed to whether or not this is physically meaningful.

Another useful space in which to represent the map is on a unit two-torus $T^2 = S^1 \times S^1$ ($p \in S^1$, $\theta \in S^1$).

$$r_{n+1} = r_n + K \sin(\theta_n) \bmod 2\pi \quad (2.4a)$$

$$\theta_{n+1} = \theta_n + r_{n+1} \bmod 2\pi \quad (2.4b)$$

This representation is especially useful when it comes to plotting the results of a mapping of a point as the area in which the point can move is finite. However, again one must pay heed to whether or not this is physically meaningful.

We will frequently use the standard map in the following form

$$p_{n+1} = p_n - \frac{K}{2\pi} \sin(2\pi\theta_n) \quad (2.5a)$$

$$h_{n+1} = h_n + p_{n+1} \quad (2.5b)$$

which is related to eqns. 2.2 by the transformation $\theta \rightarrow 2\pi h + \pi$ and $r \rightarrow 2\pi p$. Some of the figures in this report will be given in this form, e.g. fig. 2.3b.

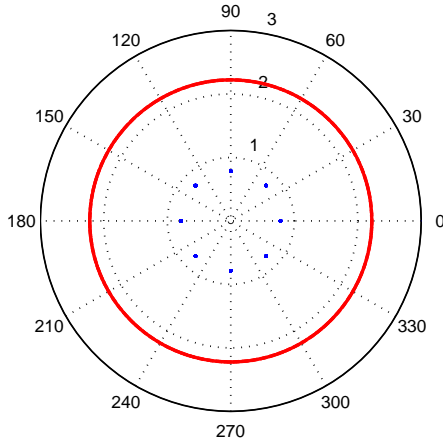
We mentioned previously that the standard map is a conservative map, or to put it another way, has a certain area-preserving property. To see this, we evaluate the Jacobian of the map and see that it is equal to +1 (we are treating each iteration of the mapping as though it is a transformation). We will

now verify this explicitly for our polar representation given by eqns. 2.2.

$$\begin{aligned} \det(J) &= \begin{vmatrix} \frac{\partial \theta_{n+1}}{\partial \theta_n} & \frac{\partial \theta_{n+1}}{\partial r_n} \\ \frac{\partial r_{n+1}}{\partial \theta_n} & \frac{\partial r_{n+1}}{\partial r_n} \end{vmatrix} \\ &= \begin{vmatrix} 1 & 1 \\ K \cos(\theta_n) & 1 + K \cos(\theta_n) \end{vmatrix} \\ &= +1 \end{aligned} \quad (2.6)$$

We should also note that as the Jacobian is positive, hence, it is not just merely area-preserving, but also, orientation-preserving (i.e. our space/area is not flipped by the transformation). Both of these properties will be of use later on. We will return to the Jacobian in a later section in order to classify fixed points in the map, but first we should examine how these fixed points arise.

Fig. 3.1 – Polar representation of the standard map with $K = 0$ for two different initial values of r iterated 1000 times. The blue points correspond to the rational circle found at $r/2\pi = 1/8$ while the red points correspond to the irrational circle found at $r/2\pi = 1/2\sqrt{2}$. See sec. 11.3 for the MATLAB script used to create this plot.



3 Near-Integrable Systems

3.1 Rotation Number

We will now consider the standard map in polar form (eqns. 2.2) when $K \neq 0$ but is “sufficiently” small. We will do this by first examining what happens when $K = 0$ and then use continuity to extend this to the K small case.

When $K = 0$ we can see from eqns. 2.2 that r is constant (i.e. $r_{n+1} = r_n$), so the mapping is purely angular; furthermore, we can see that it also twists the plane, as the angle through which the mapping takes a point is larger for larger values of r (i.e. $\theta_{n+1} - \theta_n$ is larger for larger r): see sec. 9 for further details about twist maps.

We now introduce the rotation number $\rho(r) = r/2\pi$ which allows us to quantify and explore the degree of twisting of the plane for various values of r . There are two possibilities for the value of our rotation number for various values of r :

1. The rotation number is rational for a particular value of r : $\rho(r) = r/2\pi = m/n$ where n and m are relative primes. Then every point

on the circle defined by this r is periodic under n applications of the standard map, i.e.

$$S^n : (r/2\pi = m/n, \theta_0) \longrightarrow (r/2\pi = m/n, \theta_0)$$

for all θ_0 and where S^n denotes that the standard map has been applied n times. The values of r that yield this result define the rational circles. This set of circles is dense (that is, between any two points of the set there are an infinite number of points that are also in the set) in the plane but is still denumerable.

2. The rotation number is irrational for a particular value of r . Then the mapping ergodically covers the circle, i.e. the set of points $S^l(r, \theta_0)$ ($l \rightarrow \infty$) are dense on the circle defined by this r . The values of r that yield this result define the irrational circles. This set of circles is non-denumerable.

Fig. 3.1 shows an example of illustrate and example of each of the two generic possibilities.

3.2 Fixed Points

We now consider a region near some rational surface C with $r/2\pi = m/n$ under the mapping S^n : first, consider a nearby circle C^+ with $r/2\pi > m/n$, all points rotate in an anti-clockwise direction under the mapping S^n ; now consider another nearby circle C^- with $r/2\pi < m/n$, all points rotate in a clockwise direction under the mapping S^n . Indeed, we can see that this is the case in the standard map, see figs. 11.4.

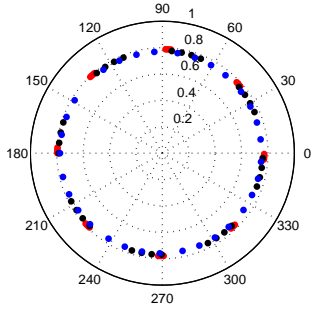
We now move on from the $K = 0$ case and consider when $K \neq 0$ but is “sufficiently” small. When $K \neq 0$ the mapping is no longer purely angular: there is now also a radial component to the mapping: however, by choosing a small enough value of K we can still maintain that all points on C^+ rotate in an anti-clockwise, and that all points on C^- rotate in a clockwise direction. Now, by continuity, we have that there must be a point between C^+ and C^- that does not change its angular location under the mapping S^n . Thus, there exists an $r = R(\theta)$ such that

$$S^n : (R(\theta), \theta) \longrightarrow (R'(\theta), \theta) \quad (3.1)$$

This set of points defines a continuous curve D which are mapped only in the radial direction under

Fig. 3.2 – Three initial conditions were iterated 32 times under the standard map for two different values of K : one with $r_{\text{black}}/2\pi = 1/8$, which lies on the rational circle $C(r/2\pi = 1/8)$; one with $r_{\text{blue}}/2\pi = 1/8.1$ which lies just outside the rational circle, and so should iterate in anti-clockwise direction for sufficiently small K ; and one with $r_{\text{red}}/2\pi = 1/7.9$ which lies just inside the rational circle, and so should iterate in clockwise direction for sufficiently small K . And indeed, we can see that this is the case in the standard map. See sec. 11.4 for the MATLAB script used to create this plot.

(a) Application to the rational circle $C(r/2\pi = 1/8)$ of the standard map with K too large: $K = 0.01$.



(b) Application to the rational circle $C(r/2\pi = 1/8)$ of the standard map with K sufficiently small: $K = 0.0001$. We can see that for radii larger than that of the rational circle we have anti-clockwise rotation while the converse is true for radii smaller than that of the rational surface.

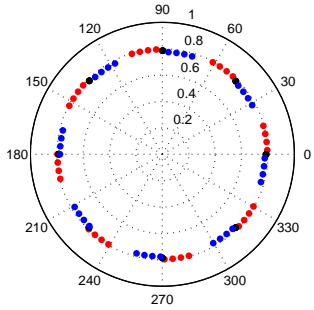
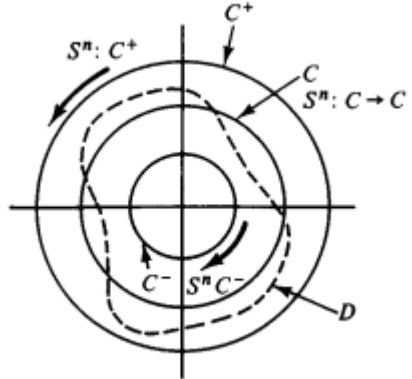


Fig. 3.3 – Region of the standard map near a rational circle C . Image taken from [1].



S^n , see fig. 3.3. If the mapping S^n has any fixed points then they must lie somewhere on D and have no movement in the radial direction under S^n , i.e.

$$S^n : (R(\theta), \theta) \longrightarrow (R(\theta), \theta) \quad (3.2)$$

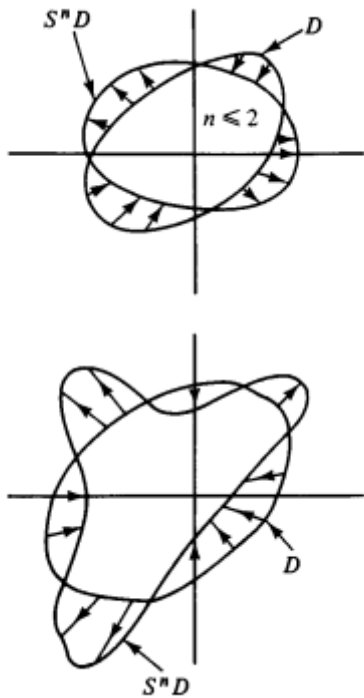
Next, we consider the curve S^nD , that is the curve D under the mapping S^n . As the mapping S^n is purely radial, we know that any intersections between S^nD and D are fixed points of S^n . It should be noted that we refer to fixed points of S^n as *fixed points of the standard map of order-n*.

The fact that the standard map is area-preserving implies that the standard map applied n times is area-preserving, i.e. S^n is also area-preserving. This means that the area enclosed by S^nD is the same as the area enclosed by D . This yields a limited number of possibilities, several of which are illustrated in fig. 3.4. We can see that the curves S^nD and D must intersect at an even number of points, as such, the mapping S^n has an even number of fixed points. This was originally conjectured by Poincaré from a consideration of the three-body problem in celestial mechanics but was proved by Birkhoff, and hence, is known as the *Poincaré-Birkhoff fixed point theorem*, or sometimes as *Poincaré last geometric theorem* (so called by Birkhoff).

The above is true for all n , however, this is not the only thing we can conclude. Let (r_0, θ_0) be a fixed point of S^n , i.e.

$$S^n(r_0, \theta_0) = (r_0, \theta_0) \quad (3.3)$$

Fig. 3.4 – Limited number of possibilities for D and $S^n D$.
Image taken from [1].



then clearly

$$S^{n+l}(r_0, \theta_0) = S^l(r_0, \theta_0) \quad (3.4)$$

for all $l \in \mathbb{N}^+$ so the points

$$S^1(r_0, \theta_0), S^2(r_0, \theta_0), \dots, S^{n-1}(r_0, \theta_0) \quad (3.5)$$

are each, also, distinct fixed points of S^n : so we can see that our mapping has *at least* n fixed points in the region of the curve C . We shall see in the next section that our mapping actually has at least $2n$ distinct fixed points in the region of the rational circle C . However, we will first need to linearise our mapping around these fixed point.

3.3 Linearisation

Recall the Jacobian

$$\begin{aligned} J &= \begin{pmatrix} \frac{\partial \theta_{n+1}}{\partial \theta_n} & \frac{\partial \theta_{n+1}}{\partial r_n} \\ \frac{\partial r_{n+1}}{\partial \theta_n} & \frac{\partial r_{n+1}}{\partial r_n} \end{pmatrix} \\ &\equiv \begin{pmatrix} J_{11} & J_{12} \\ J_{21} & J_{22} \end{pmatrix} \end{aligned}$$

A linear approximation

$$\begin{pmatrix} \theta_{n+1} \\ r_{n+1} \end{pmatrix} = \begin{pmatrix} J_{11} & J_{12} \\ J_{21} & J_{22} \end{pmatrix} \begin{pmatrix} \theta_n \\ r_n \end{pmatrix} \quad (3.6)$$

is reasonably valid near our fixed points. Next consider the eigenvectors of this map, the eigenvalues are given by the determinant

$$\begin{vmatrix} J_{11} - \lambda & J_{12} \\ J_{21} & J_{22} - \lambda \end{vmatrix} = 0 \quad (3.7)$$

For a 2×2 matrix we have that

$$\lambda^2 - \text{tr}(J) + \det(J) = 0 \quad (3.8)$$

From eqn. 2.6 we have that $\det(J) = 1$, thus the so-called *characteristic multipliers* of the map at a fixed point are given by

$$\lambda = \frac{1}{2} \left[\text{tr}(J) \pm \sqrt{(\text{tr}(J))^2 - 4} \right] \quad (3.9)$$

So, we can see that the eigenvalues of J are completely determined by its trace, which we will see is an important property later in our analysis. Now since the two eigenvalues satisfy $\lambda_1 \lambda_2 = \det(J) = 1$. We have two cases:

1. λ_1 and λ_2 are both real with $|\lambda_1| \geq 1$ and $|\lambda_2| = |1/|\lambda_1|| \geq 1$.
2. λ_1 and λ_2 are both complex conjugates of the form $\lambda_1 = \exp(i\phi)$ and $\lambda_2 = \exp(-i\phi)$ for some $\phi \in \mathbb{R}$.

In case 1, the fixed point is a *hyperbolic point*. This can be seen explicitly by examining the eigenvalues: $|\lambda_1| \geq 1$, so repeatedly applying our mapping will move any points near the corresponding eigenvector *outward* from the fixed point, along that eigenvector; whereas $|\lambda_2| = |1/|\lambda_1|| \geq 1$, so repeatedly applying our mapping will move any points near the corresponding eigenvector *inward* towards the fixed point, along that eigenvector.

In case 2, we have an *elliptic point*. Our complex eigenvalues correspond to a rotation, however, the two eigenvalues, in general, have different magnitudes; hence we have an elliptic rotation rather than circular rotation (we have circular rotation in the special case where we have purely imaginary numbers for the two complex conjugate eigenvalues). It is important to note that these curves are

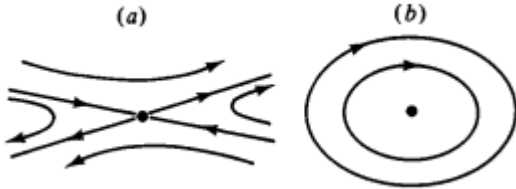


Fig. 3.5 – Hyperbolic fixed point (a); elliptic fixed point (b)

not the same as the flow lines in a continuous phase space since the points are related by a discrete map.

The fact that we have hyperbolic and elliptic fixed points is not at all surprising when we go back and examine figs. 3.3 and 3.4. By combining these two figures we can ascertain the global behaviour of our map in the region of the rational circle C : from this, we can directly see our hyperbolic and elliptic fixed points (see fig. 3.6). Since the “flow” of the map S^n is anti-clockwise (and also radial) outside D and $S^n D$ and clockwise inside them, it is clearly seen that the flow generated by S^n near the fixed points is either hyperbolic or elliptic. From this we can also see that these fixed points appear in alternating pairs, a feature which is not apparent from the local analysis but is apparent from considering the global scale.

We now note that, as hyperbolic flows are not topologically equivalent to elliptic flows, nor are they vice-versa, it follows that hyperbolic fixed points cannot be mapped into elliptic fixed points, or vice-versa. Thus, there are $2n$ fixed points of S^n in the region of the rational surface C : as was claimed previously. Further still, we have only been considering the region near the rational circle C : however, more than just one rational curve exists in our mapping S^n . Hence there are always $2nl$ fixed points of S^n , where $l \in \mathbb{Z}$.

So, to summarise our results thus far:

All rational circles ($r/2\pi = m/n$) which were invariant curves under S , if $K = 0$, do not go into invariant curves if $K \neq 0$. Rather, they are “destroyed”, in the sense that S^n only has *isolated fixed points rather than invariant curves*. Thus, any perturbation method for calculating the change in C ($r/2\pi = m/n$) due to a change in K from $K = 0$ will diverge.

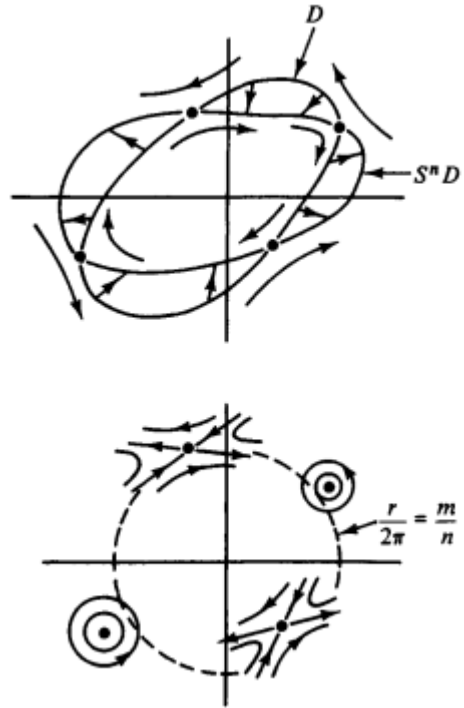


Fig. 3.6 – Location of the two types of fixed points on the curves D and $S^n D$.

We will now consider aspects of each of the two types of fixed points in our mapping separately, starting with hyperbolic fixed points before then moving onto elliptic fixed points. We will then finally put the two together to obtain what we require.

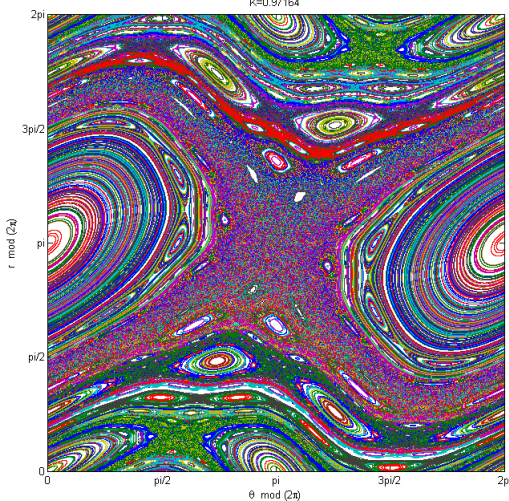


Fig. 4.1 – First order hyperbolic fixed point of the standard map for $K = 0.9716$. See sec. 11.1 for the MATLAB script used to create this plot.

4 Hyperbolic Fixed Points

4.1 Invariant Curves

We consider the hyperbolic fixed point, denoted x_0 , of an area-preserving map S (i.e. replacing the standard map with a general area-preserving map S , e.g. the twist map of sec. 9: only the area-preserving property is important for the following arguments). The eigenvectors of the linear approximation (the Jacobian) are tangent to the invariant curves of the full non-linearised map at the hyperbolic fixed point x_0 . However, we have not yet defined these invariant curves; but we shall do so now.

These curves are the set of points which are either mapped asymptotically to a hyperbolic fixed point x_0 by S^n or S^{-n} as n tends to infinity.

Specifically, we have the stable manifold W^s which is defined to be the set

$$W^s = \left\{ x \mid \lim_{n \rightarrow \infty} S^n x = x_0 \right\} \quad (4.1a)$$

whereas the unstable manifold W^u is the set

$$W^u = \left\{ x \mid \lim_{n \rightarrow \infty} S^{-n} x = x_0 \right\} \quad (4.1b)$$

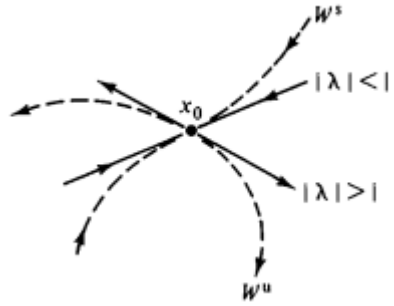


Fig. 4.2 – Hyperbolic Fixed Point. Image taken from ref. [1].

As we already stated, these smooth sub-manifolds are tangent to the eigenvectors with $|\lambda| < 1$ or $|\lambda| > 1$ respectively, see fig. 4.2.

What is the behaviour of these sub-manifolds away from the immediate neighbourhood of the hyperbolic fixed point? That is, if $x \in W^u$, where does $S^n x$ go as $n \rightarrow \infty$ or if $x \in W^s$, where does $S^{-n} x$ go as $n \rightarrow \infty$? One possibility is for two distinct fixed points of S , labelled a and b , to share their stable manifolds, W^s , and unstable manifolds, W^u , as shown in fig. 4.3a. Of course, what is stable for one is unstable for the other. The second possibility is for the unstable manifold of a fixed point a to loop back towards a and become the stable manifold, forming a closed loop, as shown in fig. 4.3b.

It can be shown that an impossible situation is for a manifold to cross itself, as such a crossing would violate our continuity condition (see [1]). Instead, the generic situation is for W^s to cross a manifold W^u which is connected with either the same hyperbolic fixed point, or with another one. These possibilities are shown in fig. 4.4a. If the manifolds W_b^s and W_b^u , which are associated with the same fixed point b , have a point in common, it is called a *homoclinic point*. On the other hand, if W_a^s and W_b^u , which are each associated with two distinct fixed points a and b respectively, have a point in common, it is called a *hetroclinic point*. Both types of point are present in fig. 4.4a. In fact, if we examine fig. 4.4a, we see that there is more than one of each type of point present. This is because Poincaré recognised that if there is one such homoclinic or hetroclinic point there is an infinite number of such points. Thus, for fig. 4.4a

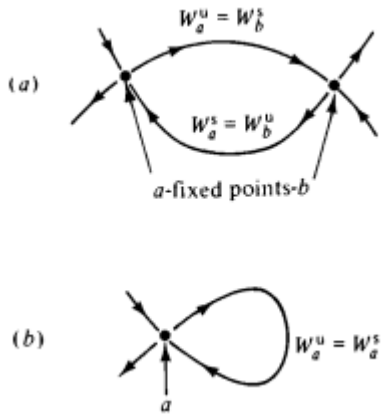
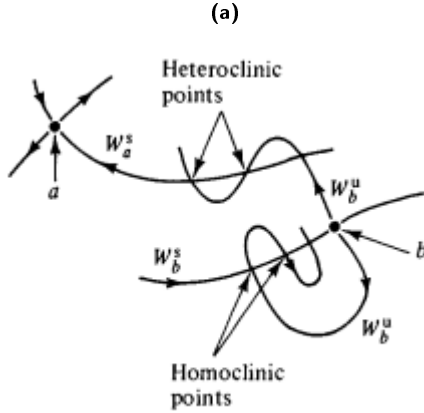


Fig. 4.3 – The two possibilities for the stable W^s and unstable W^u manifolds away from the hyperbolic fixed point(s). Image taken from [1].

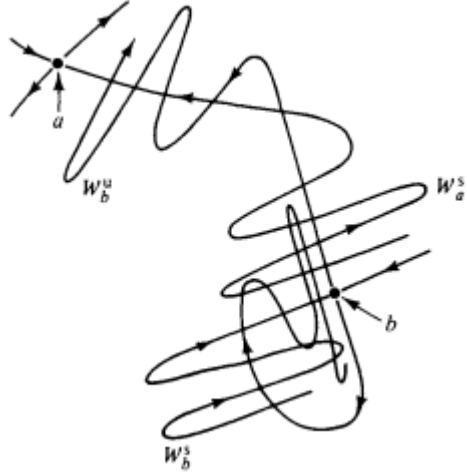
to be more complete, but not totally complete, it aught to look more like fig. 4.4b.

As bad as this looks it does not even begin to do justice to the complexity, because not only must there be an infinite number of homoclinic points, but W^u and W^s must oscillate more and more wildly (in phase space) between each of the homoclinic points, the beginnings of which can be seen in fig. 4.4a. This has a further implication: between any two homoclinic points, say x_0 and x_0^* , there must be a dense set of intersections of W^u and W^s . Similarly, a dense set of intersections exist on W^s between x_0^* and $x_1 = Sx_0$. By dense, we mean that in any portion of W we can find an intersection. This fact can be proved rigorously using the area and the orientation preserving properties of our map (see [1]). However, it can be seen figuratively by first considering a limited number of homoclinic points, around which the oscillations W^u and W^s are relatively small, see fig. 4.5a. Now, consider more and more of this infinite set of homoclinic points: as more of these points are considered, the oscillations (in phase space) become wilder. We now see, that as our manifolds cannot cross themselves, these oscillations must entwine themselves in an increasingly complicated manner, contrast fig. 4.5b with fig. 4.5a. Each of these entwinements introduces extra intersections between W^s and W^u , which, for example, can be seen along the green section of fig. 4.5b

Fig. 4.4 – Generic possibilities for W^s and W^u away from the hyperbolic fixed point(s). Images taken from [1].



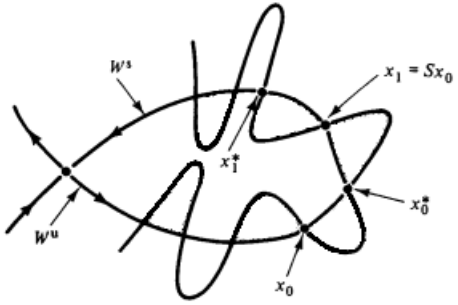
(b) Is a more, but far from totally complete, version of fig. 4.4a.



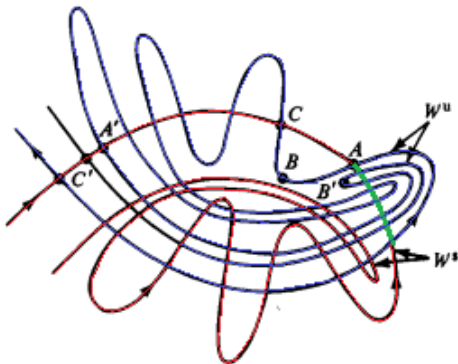
This winding is indicative of the existence of Smale horseshoes, that is, a folding of our phase space back upon itself multiple times. It can be claimed that, this winding structure, these Smale horseshoes, will produce chaotic dynamics. The areas of our phase space in which this winding occurs should coincide with the chaotic areas of our phase space.

Fig. 4.5 – Oscillations of the manifold around homoclinic points. Images are modified versions of images taken from [1].

(a) A limited number of homoclinic intersections of W^s and W^u near a hyperbolic fixed point.



(b) More homoclinic intersections leading to an increasingly complicated entwinement of W^s and W^u and more and more intersections between the two manifolds, which can be seen particularly well along the green section of W^s . Note: (A, B, C) have been mapped after 3 iterations to (A', B', C').



4.2 Invariant Curves in the Standard Map

Our arguments up to this point have been about hyperbolic fixed points in a general area preserving map. We will now confirm the existence of these stable and unstable manifolds in the standard map numerically. Recall the eigenvectors of the linear approximation (the Jacobian) are tangent to the invariant curves (the stable W^s and unstable W^u manifolds) of the full non-linearised map at the hyperbolic fixed point x_0 . Knowing this, we will proceed as follows

1. Calculate the (first order) fixed points of our map.
2. Calculate the Jacobian around each of the fixed points.
3. Calculate the eigenvalues and corresponding eigenvectors of the fixed points from the Jacobian; classify the fixed points and select the hyperbolic fixed point.
4. Knowing that the eigenvectors of the linear approximation (the Jacobian) are tangent to the invariant curves at this fixed point, and in particular, that the eigenvector corresponding to the eigenvalue $|\lambda| > 1$ is tangent to the unstable manifold W^u at this fixed point; we will select a dense set of points (up to what is computationally feasible) that lie on this eigenvector close to the fixed points. This gives us a set of points that lie on, or at least are very close to lying on, the unstable manifold. We will then apply our mapping repeatedly to each of these points, which will each remain on, or very close to on, the unstable manifold. This whole process enables us to be able to see the path of the unstable manifold through our phase space.

4.2.1 (First order) Equilibrium points of our Map

As we want to be able to plot the results, we will consider the map on a unit two-torus, i.e. eqns. 2.4. At a first order fixed point $\theta_{n+1} = \theta_n$ and $r_{n+1} = r_n$, thus

$$r_n = r_n + K \sin(\theta_n) \mod 2\pi \quad (4.2a)$$

$$\theta_n = \theta_n + r_n \mod 2\pi \quad (4.2b)$$

which becomes

$$\theta_n = k\pi \mod 2\pi \quad (4.3a)$$

$$0 = r_n \mod 2\pi \quad (4.3b)$$

where $k \in \mathbb{Z}$.

$$\theta_n - k\pi = 2\pi l \quad (4.4a)$$

$$r_n = 2\pi n \quad (4.4b)$$

where $n, l \in \mathbb{Z}$. Which give us our fixed points

$$\bar{\theta} = \pi m \quad (4.5a)$$

$$\bar{r} = 2\pi n \quad (4.5b)$$

where $m \equiv (2l + k) \in \mathbb{Z}$. Thus there are 2 distinct first order fixed points on our toroidal representation.

4.2.2 Calculating the Jacobian for each Fixed Point

We now calculate out the linearisation of our map around the fixed points. Recall the Jacobian, which at our fixed points is given by

$$J(\bar{\theta}, \bar{r}) = \begin{pmatrix} 1 & 1 \\ K & 1 + K \cos(\bar{\theta}) \end{pmatrix} \quad (4.6)$$

$$= \begin{cases} \begin{pmatrix} 1 & 1 \\ 1 & 1+K \end{pmatrix} & \text{for } m \text{ even} \\ \begin{pmatrix} 1 & 1 \\ -K & 1-K \end{pmatrix} & \text{for } m \text{ odd} \end{cases} \quad (4.7)$$

4.2.3 Classification of fixed points

The eigenvalues are given by eqn. 3.9, thus

$$\lambda = \begin{cases} \frac{1}{2} [2 + K \pm \sqrt{K^2 + 4K}] & \text{for } m \text{ even} \\ \frac{1}{2} [2 - K \pm \sqrt{K^2 - 4K}] & \text{for } m \text{ odd} \end{cases} \quad (4.8)$$

Using the conditions in sec. 3 we find that the m odd case yields elliptic fixed points while the m even case yields the desired hyperbolic fixed points (provided $K < 4$). Thus, from eqns. 4.5 we see that there is one elliptic and one hyperbolic (first order) fixed point on our toroidal representation (when $K < 4$).

4.2.4 The Unstable Manifold

Figs. 4.6 show the result of applying the mapping 17 times to a dense set of points (up to what is computational practical) that are initial on the eigenvector corresponding to the unstable eigenvalue and as such are on, or at least are extremely close to being on, the unstable manifold W^u of a first order hyperbolic fixed point of the standard map². It should be noted that phase of our map has been shifted so that the first order hyperbolic fixed point is now in the very centre of the plots: it is more difficult to see the behaviour near the fixed point if we

do not perform this phase shift, as the regions of our plots that are nearest to the fixed point are the four corners of each of our plots. We see that after 17 iterations the initial line of points is now quite smeared out. In fact, if we continue to iterate the points become so smeared out that we cannot discern one curve from another. So we can no longer see where the unstable manifold W^u has taken our points: we cannot map out the unstable manifold any further. We can try and combat this problem by upping the numerical density of our initial set of points, however, this only (slightly) increases the number of iterations we can perform before our method breaks down.

4.3 StdMap

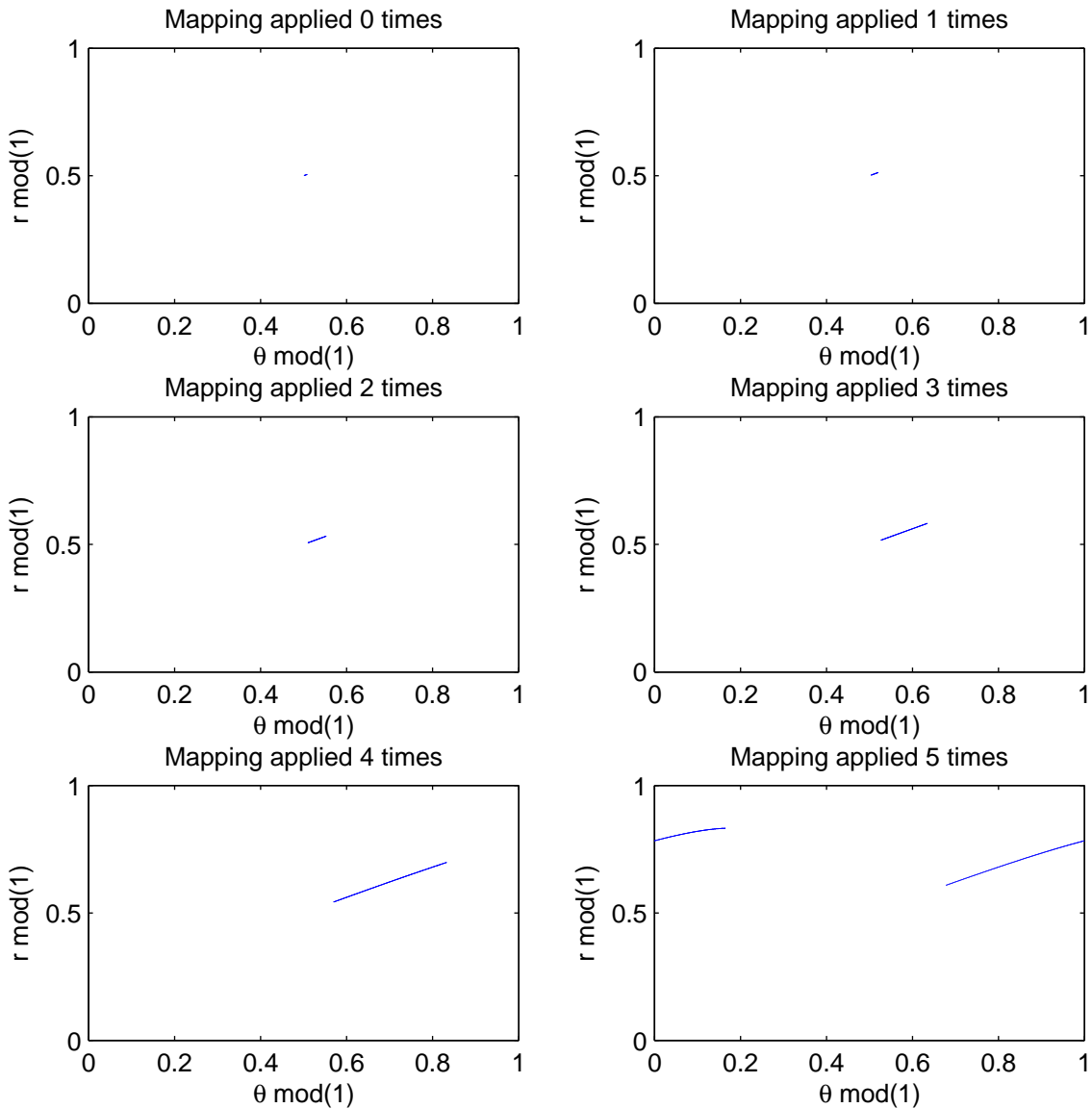
We will now employ the use of a program called *StdMap*, available from [3]. *StdMap* is a small program for Macintosh computers that allows you to explore the dynamics of a dozen or so reversible, area-preserving mappings, including the standard map. *StdMap* uses an algorithm suggested by [4] to efficiently calculate the invariant manifolds of a map. *StdMap* calculates the stable W^s and unstable W^u manifolds to a much greater resolution and compensates for the smearing problem: as such, the *StdMap* can give us continuous curves rather than a set of points for the manifold. *StdMap* actually calculates both the unstable W^u and stable W^s manifolds simultaneously, which are plotted as red and blue curves respectively. However, first we should note two points: firstly, the initial conditions *StdMap* iterates to calculate the manifolds is not the same as our initial conditions, as such, we may find that the winding structure is encountered after more, or less iterations than in our program; secondly, the phase of the plots from *StdMap* differ from ours. *StdMap* does not have the option of adjusting the phase so that the hyperbolic fixed point is in the centre of our plots, rather, the best that could be achieved with *StdMap* was to have the hyperbolic fixed point half way up the side of the plots. Figs. 4.7 show the result of the mapping up to 30 iterations. The complexities of the pictures were first envisioned by Poincaré who famously said:

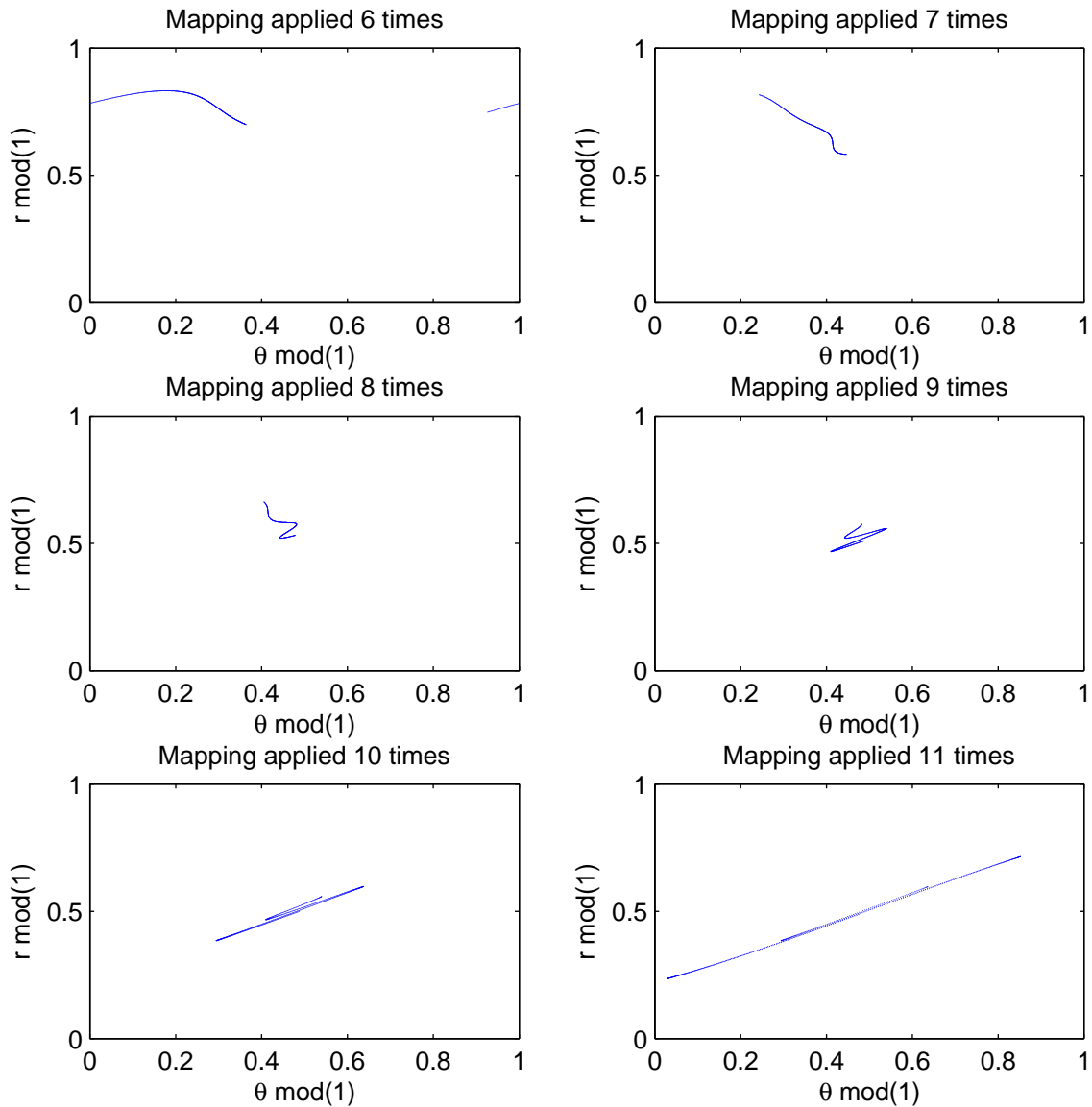
When one tries to depict the figure formed by these two curves and their infi-

² Here we are finding the unstable manifold W^u . However, using the fact that our map is time reversible one could just as equally find the stable manifold W^s .

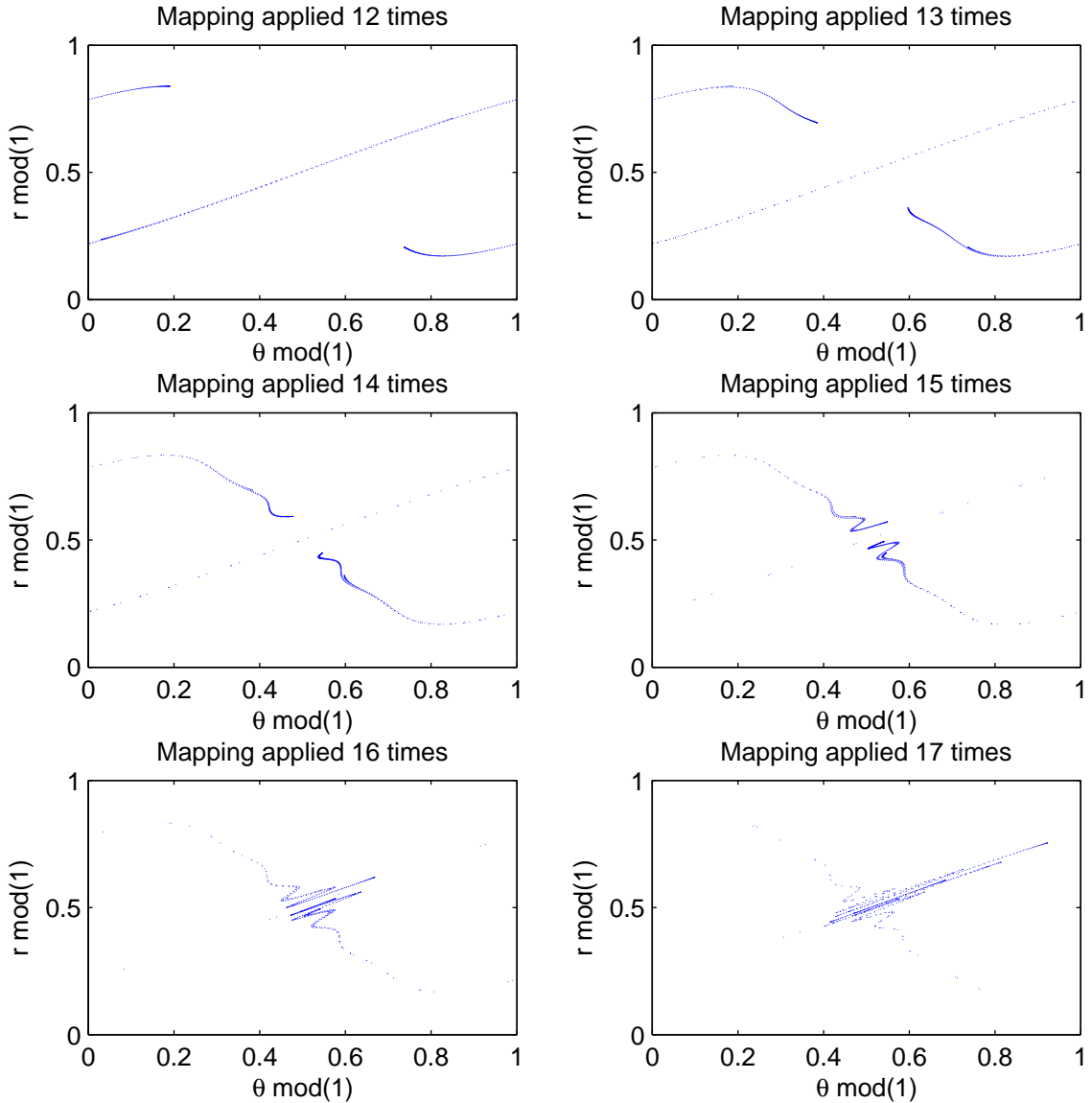
Fig. 4.6 – The complexity of the unstable manifold. See sec. 11.5 for the MATLAB script used to create these plots.

(a) We can see (barely) that points are initially a very tight line of points near the hyperbolic fixed point at $(0.5, 0.5)$. As the map is applied our points move out along the unstable manifold W^u , and are smeared out along the manifold as the further a point is from the fixed point the quicker it moves along the manifold.





(b) The points continue along the unstable manifold W^u , but now the manifold is approaching the hyperbolic fixed points (remember the points are on a torus). However, as the points approach the hyperbolic fixed point, they start to oscillate in a wilder manner.



(c) The points eventually oscillate so wildly that they start to approach the hyperbolic fixed point again. The process repeats itself, and so we have winding upon winding. We should also note that after 17 oscillations the points are now quite smeared out.

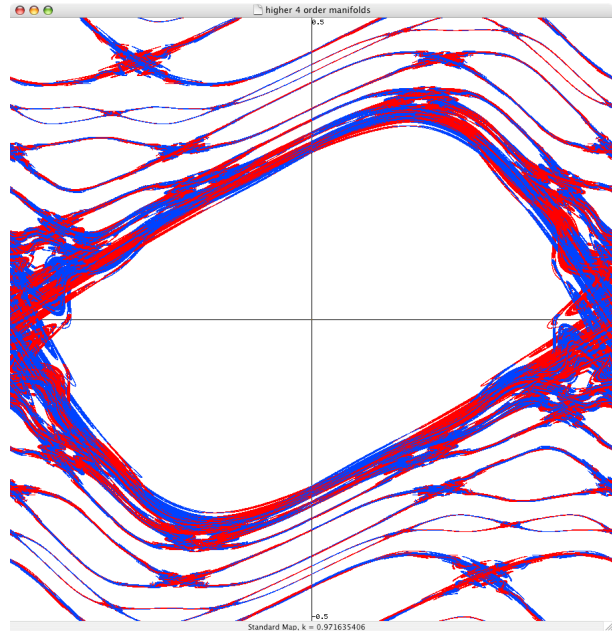
mity of intersections, each of which corresponds to a doubly asymptotic solution, these intersections form a kind of net, web or infinitely tight mesh; neither of the two curves can ever cross itself, but must fold back on itself in a very complex way in order to cross the links of the web infinitely many times. One is struck by the complexity of this figure that I am not even attempting to draw. (see [5])

Up to now we have only considered the first order fixed points of our map, however, we know that fixed points of higher orders exist. We can repeat the arguments of sec. 4.2 except instead identifying first order fixed points, we identify higher order fixed points. However, StdMap allows us to easily obtain the stable and unstable manifolds corresponding to higher order hyperbolic fixed points. Figs. 4.8 show the stable W^s and unstable W^u manifolds for hyperbolic fixed points up to the order given under each plot.

However, perhaps what is most interesting is when we compare the locations of these manifolds to the results of many iterations, of many different initial conditions of the Standard map. From this, we can see that the earlier claim, that the areas of our phase space which contain these winding manifolds will coincide with the chaotic regions of our phase space, seems to be justified: see figs. 4.9. Note, that we have done shown this here for a particular value of $K = 0.97164$ but that this comparison will hold for all values of K .

Fig. 4.9 – Comparison of these figures shows that the stable and unstable manifold coincide with the chaotic regions of our phase space. These plots have been created using StdMap [3].

(a) The stable and unstable manifolds.



(b) Many iterations of our mapping for the same value of K .

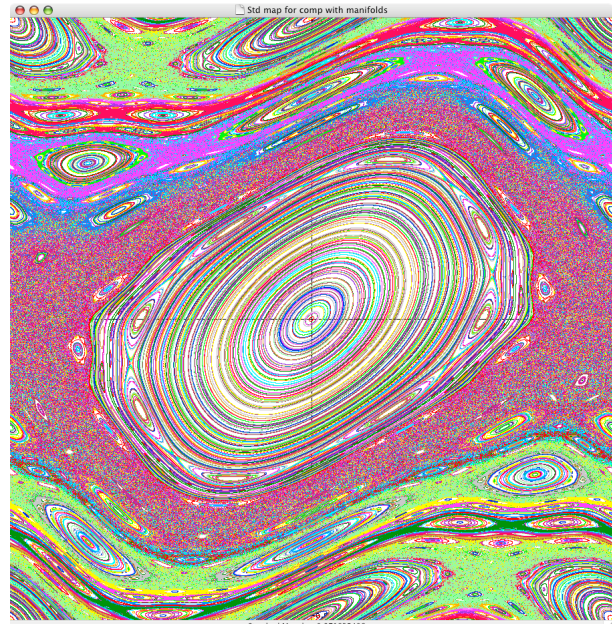


Fig. 4.7 – The complexity of the stable (blue) and unstable (red) manifolds. The complexity of the stable (blue) and unstable (red) manifolds [invariant curves]. These plots have been created using StdMap [3].

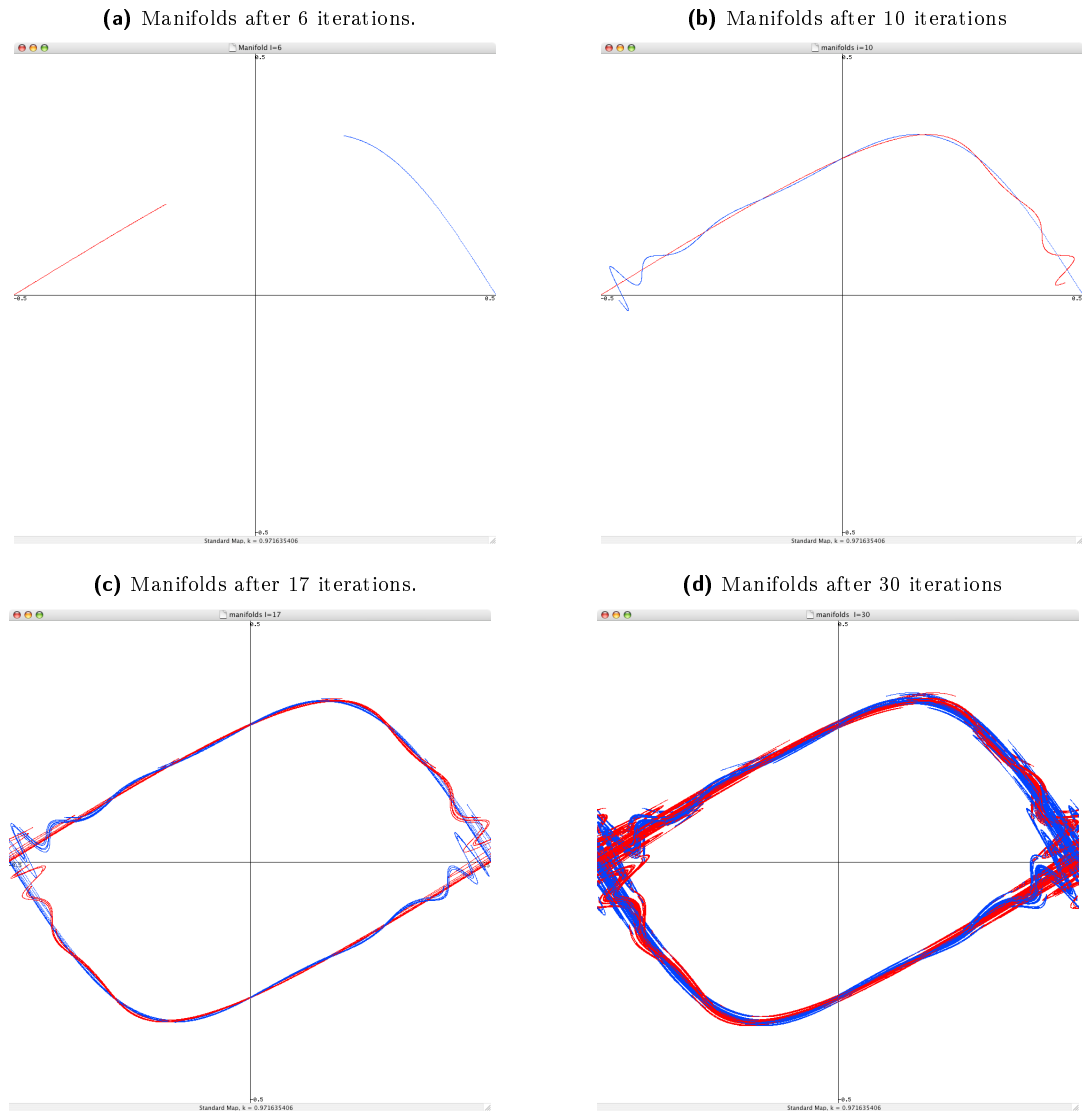
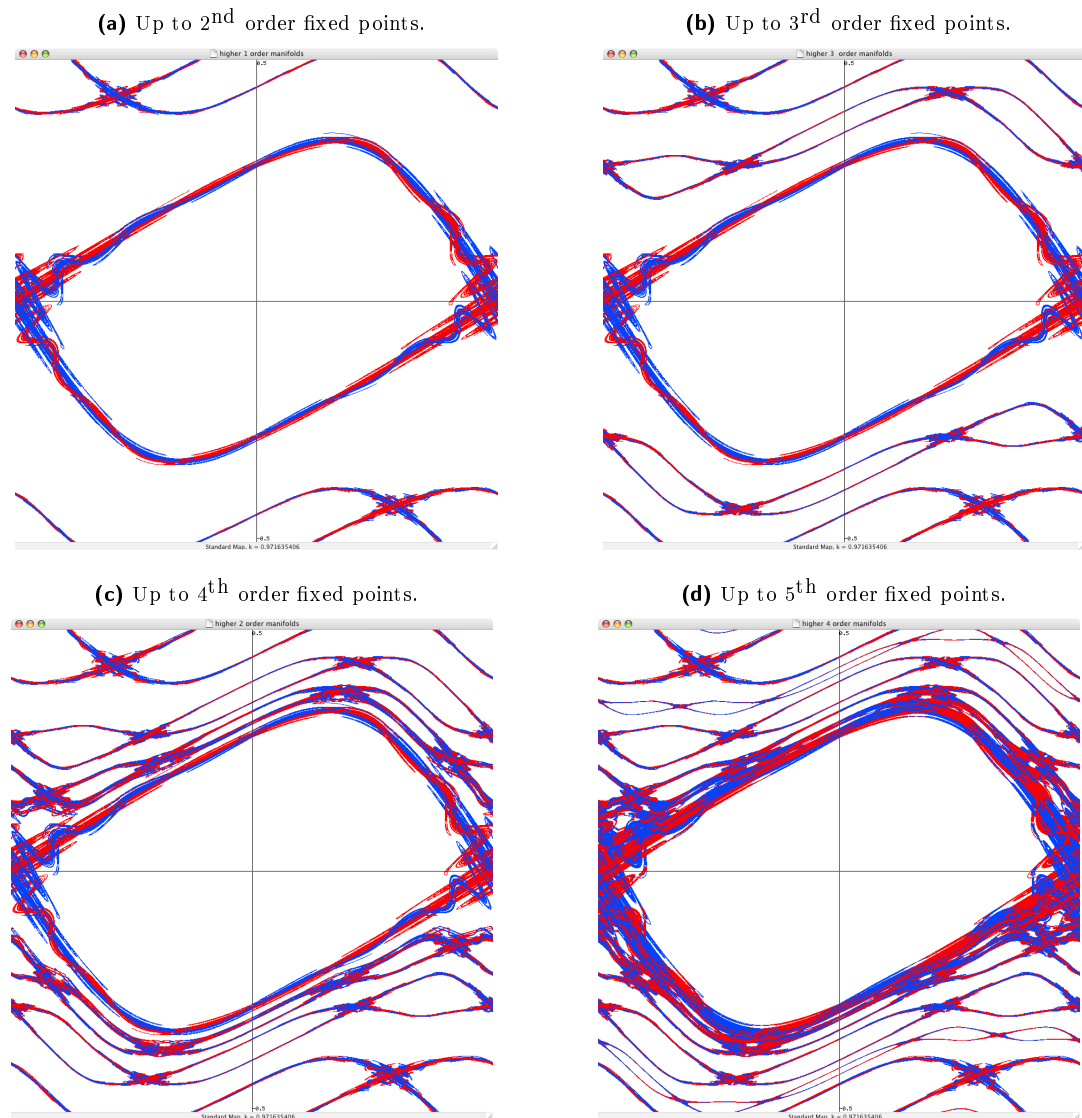


Fig. 4.8 – The invariant curves of the standard map up a certain order. These plots have been created using StdMap [3].



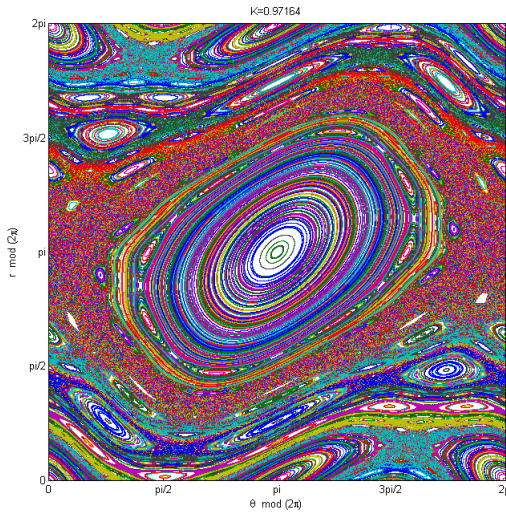


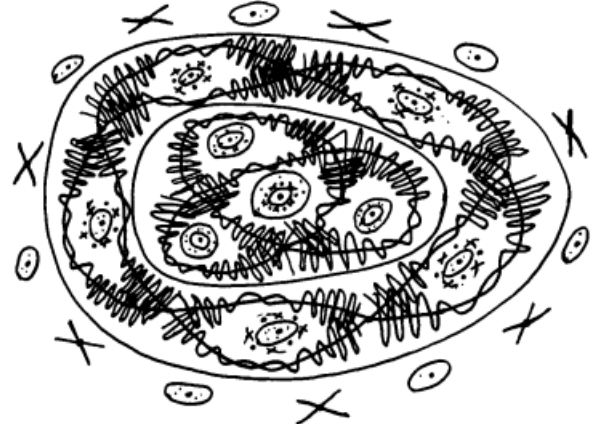
Fig. 5.1 – First order elliptic fixed point of the standard map for $K = 0.9716$. See sec. 11.1 for the MATLAB script used to create this plot.

5 Elliptic Fixed Points

5.1 Microcosms within Microcosms

The prior section gives us a vague idea of the complexity of area-preserving maps near hyperbolic fixed point. In this section, we ask, what occurs near an elliptic fixed point? It has been shown by Arnold and Moser [2] that around the elliptic fixed points, for sufficiently small K in the standard map, or, more generally in the twist map, there are closed curves which are covered densely by the iterates of the map S^n ($n = 1, 2, \dots$). These invariant closed curves about the elliptic fixed points are isolated from each other. Zehnder [2] has shown that between any two such invariant curves are both hyperbolic and elliptic fixed points of some higher order. That is, if the elliptic fixed point is a fixed point of order n , i.e. a fixed point of the mapping S^n , then around it, but between a pair of these invariant closed curves, are elliptic and hyperbolic fixed points of order $n \cdot m$, i.e. a fixed point of the map $(S^n)^m$. What this means is that we obtain a microcosm of what occurs for the original system of rational and irrational curves. Around each of these secondary elliptic fixed points is yet another set of elliptic and hyperbolic fixed points of even higher order, $n \cdot m \cdot p$, i.e. a fixed point

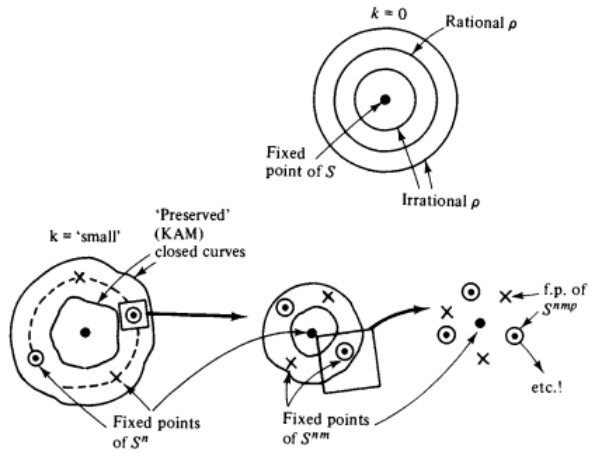
Fig. 5.2 – Microcosm's within microcosms: depiction of a complexity that even Poincaré was reluctant to attempt to draw. Image taken from [1].



of the mapping $((S^n)^m)^p$. This process of building microcosms within microcosms continues indefinitely.

Despite the “infinity complexity”, a number of people have tried to characterise it, indeed fig. 5.2 doesn’t even come close to the actual complexity, since there is no way to illustrate dense sets of preserved and broken $K = 0$ surfaces. We can in actual fact see this complexity in the standard map with relative ease, see figs. 5.4.

Fig. 5.3 – Break-up of rational curves into fixed points and the preservation of some irrational surfaces as KAM curves. Image taken from [1].



Thus, around the original fixed point of S , the

circles with rational rotation numbers break up into hyperbolic and elliptic fixed points. However, for sufficiently small K , some of the circles are only slightly perturbed and remain closed curves which are covered densely by iterates of S , see fig. 5.3. These “preserved” closed curves are known as *KAM curves* (*Kolmogorov-Arnold-Moser*).

5.2 Numerical Example

To be more specific, let us consider the standard map specifically with some numerical examples. We wish to determine the fate of some KAM curves as K is increased. In actual fact we should, in the numerical cases, refer to them as “KAM curves” because while they may appear to be smooth lines in a numerical example, in actual fact we may not have smooth, connected curves at all, but rather a series of islands too small to be numerically resolved. Figs. 5.5 show the behaviour of eight different initial conditions under 10,000 iterations of the standard map³ (of the form of eqns. 2.5) for various values of K . The eight different initial conditions are given by the following

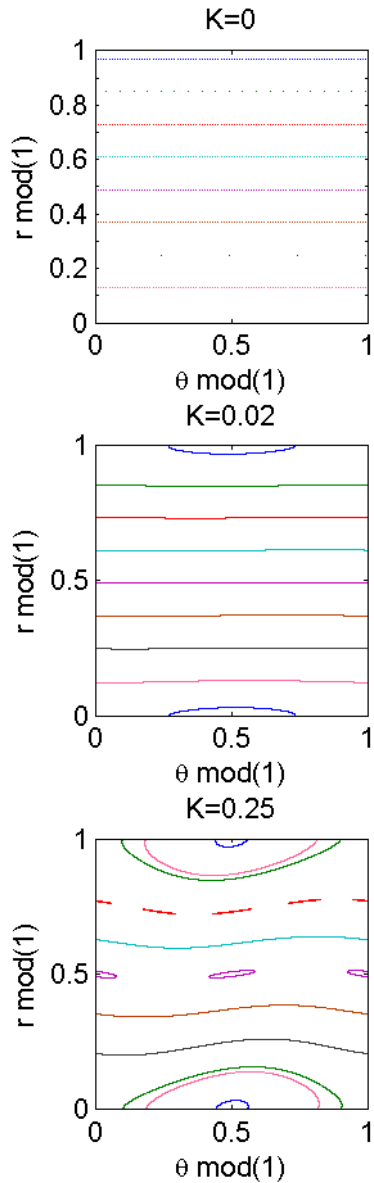
$$(r_0 = 0.97 - 0.12n, \theta_0 = 0.49) \quad n = 0, 1, \dots, 7$$

in order to evenly distribute the eight sets of points in our phase space.

When $K = 0$, our mapping is purely angular, and as such, the iterations are constrained along horizontal lines. We can see that the $n = 1$ (green) initial condition has period 20, while the $n = 6$ (black) has period 4. All of the other r_0 values are periodic, since they are rational, however they are barely resolved on this plot. At this point, all of these orbits lie on the main KAM curves defined by the same value of r_0 and $0 < \theta \leq 1$, i.e. $\{p, q \mid p = p_0, 0 < \theta \leq 1\}$. We shall see later, that the KAM curves cover our phase space ergodically when $K = 0$.

Changing K only slightly ($K = 0.02$), takes the orbit with $n = 0$ (blue) off this main set of KAM curves, because it no longer maps across the entire angular interval $0 < \theta \leq 1$. Note: that the top and bottom blue curves are connected on T^2 . All the other orbits now appear to ergodically cover

Fig. 5.5 – The standard map for various values of K . See sec. 11.6 for the MATLAB script used to create this plot.



(a) $n = 0$ blue; $n = 1$ green; $n = 2$ red; $n = 3$ cyan;
 $n = 4$ purple; $n = 5$ brown; $n = 6$ black; $n = 7$ pink.

³ In this form, our rational and irrational circles of the $K = 0$ case are horizontal lines.

continuous lines extending across the entire angular interval $0 < \theta \leq 1$, and so iterate on the main KAM curves.

Raising K to $K = 0.25$ we can see that the $n = 2$ (red) now resides on a set of four islands, whereas the $n = 4$ (purple) iterates on two islands. As such, these orbits clearly no longer reside on the main KAM curves. Also, we can see that we now have three single islands corresponding to $n = 0$ (blue), $n = 1$ (green) and $n = 7$ (red). We can also see that the island $n = 7$ (red) resides between $n = 0$ (blue) and $n = 1$ (green) on T^2 .

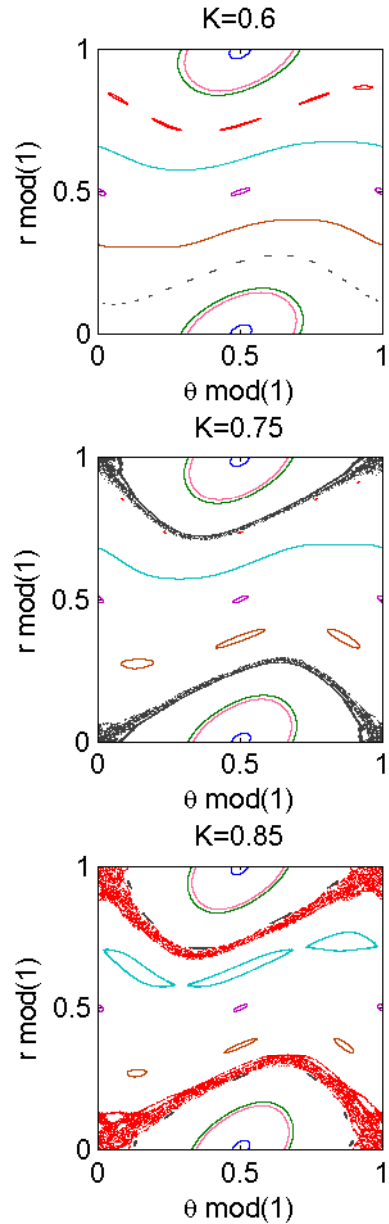
Continuing to raise K to $K = 0.6$ causes the orbit $n = 6$ (black) to iterate along 16 islands, but two orbits, $n = 3$ (cyan) and $n = 5$ (brown), still appear to be on the main KAM curves.

Raising K further still, to $K = 0.75$, only the $n = 3$ (cyan) orbit appears to remain on a main KAM curve. The $n = 6$ (black) orbit has now become a chaotic set, while the $n = 2$ set has moved onto a set of six islands, which are difficult to resolve beside the chaotic $n = 6$ (black) set.

Finally, when $K = 0.85$, the $n = 3$ (cyan) orbit now also iterates on three islands: none of our orbits are on a main KAM curve. This, of course, does not mean that there are no remaining main KAM curves left for $K = 0.85$, but rather, if there are any main KAM curves left then our points certainly do not happen to be upon them.

A point should be noted at this point however: we can see no *main* KAM curves, that is KAM curves that span across the entire angular interval $0 < \theta \leq 1$. KAM curves still exist in our phase space, as iterations to not wander freely throughout the whole phase space, and in particular, we can see that some orbits are bound along certain curves, for example, the orbits $n = 0$ (blue), $n = 1$ (green) and $n = 7$ (pink) iterate on islands associated with the 1st order elliptic fixed point. Thus, the global properties of chaotic motion is not simply a question of the preservation of the main KAM curves. The distinction between the two KAM sets is that they do not continuously deform into each other as K is varied.

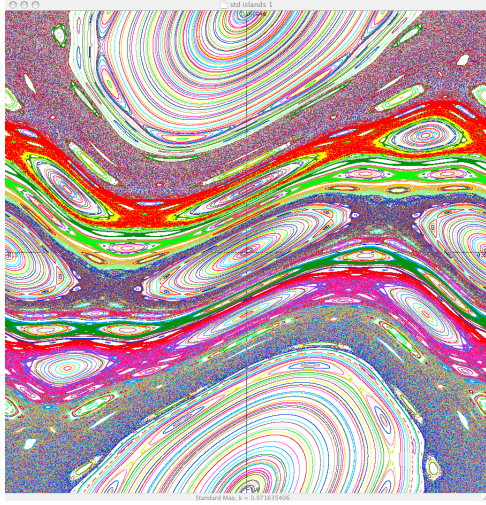
Having now seen some numerical results, let us now try to describe what has happened in this example, and later, try to consider some methods to determine the value of K which destroys a KAM surface.



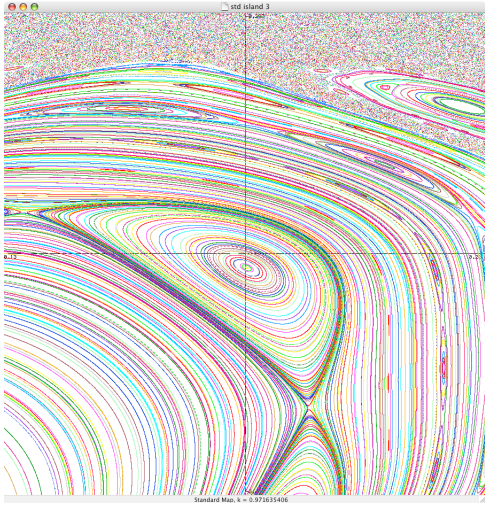
(b) $n = 0$ blue; $n = 1$ green; $n = 2$ red; $n = 3$ cyan; $n = 4$ purple; $n = 5$ brown; $n = 6$ black; $n = 7$ pink.

Fig. 5.4 – Microcosms-within-microcosms in the Standard map. These plots have been created using StdMap ([3]).

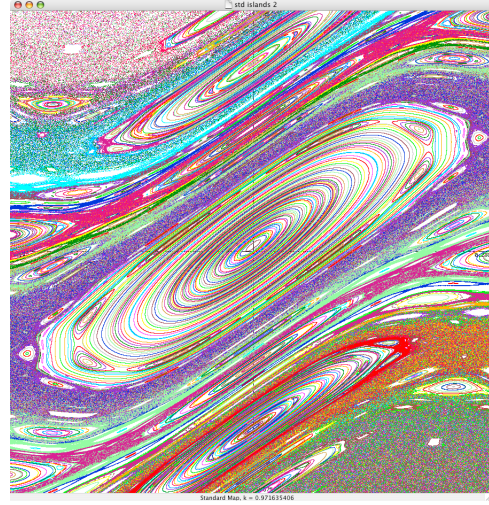
(a) The full standard map for $K = 0.971635406$. Note in particular the two second order elliptic fixed points, both of which lie on the horizontal centre line.



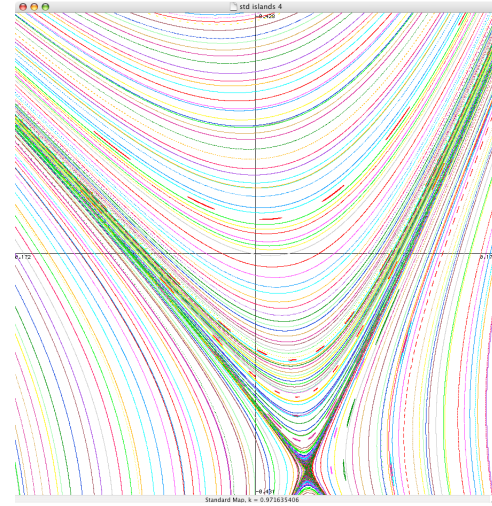
(c) “Zooming-in” further still upon the 16th order fixed points we can now very clearly see both a 16th order elliptic fixed point and a 16th order hyperbolic fixed point.



(b) Here we have “zoomed-in” a second order elliptic fixed point. Within the invariant curves surrounding it we can clearly see higher order fixed points. In particular, the eight higher order fixed points surrounding the second order fixed point. These are some of the 16th order elliptic fixed points of the standard map.



(d) “Zooming-in” further still confirms the existence of even higher order elliptical fixed points within the invariant curve of a 16th order elliptic fixed point. This seems to verify the microcosm’s-within-a-microcosm picture exists within the standard map.



6 KAM Theory

Note: This section is strongly based on [1], to the point that pieces of this section are *directly* taken from it. The aim was to order and present the arguments in [1] in a manner that suited our purpose.

6.1 The Importance of KAM Curves

The study of KAM curves is not solely based on abstract interests, but is tied into a variety of physical questions related to the possible irreversibility, diffusive or ergodic behaviour of various physical systems. The mathematical idea is quite simple. If there exists a closed invariant curve (i.e., a closed, one-dimensional, continuum of points which maps onto itself), then this curve divides \mathbb{R}^2 into two disjoint regions, namely the inside and outside regions this closed curve. The dynamical importance is that a point in the interior region cannot map onto a point in the exterior region, or vice versa. To see that this is true consider the following.

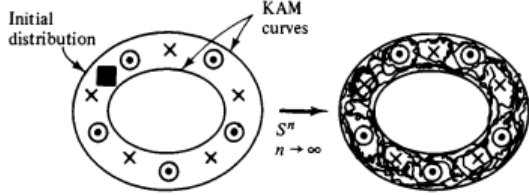
For $k = 0$, all interior points map into the interior, so for the contrary to happen for some $k \neq 0$ for which that KAM surface still exists, requires an intermediate value of k such that the interior point maps onto the KAM curve. However, since the KAM curve is invariant, and our map is time reversible (i.e. has a unique inverse map), the interior point cannot map onto it. Thus, this curve indeed divides \mathbb{R}^2 into two disjoint regions.

Therefore, while a point in the phase space may be mapped in a very erratic fashion around hyperbolic points, this erratic motion will be confined to be inside, or outside of any existing KAM curves, as schematically illustrated in fig. 6.1a and 5.2. This means that the dynamics, while erratic, is highly restricted in the phase space. In particular, if we consider a group of nearby initial states, they can only spread out in a diffusive fashion between preserved KAM curves. Such a physical system retains a significant amount of correlation with its initial state.

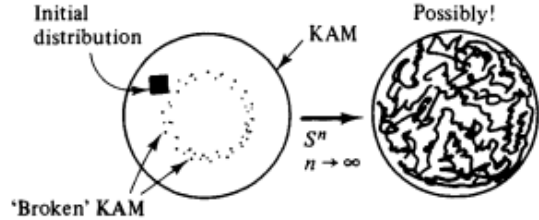
On the other hand, when a KAM curve is breaks up and ceases to be a continuum, then there is no longer an inside-outside restriction on the mapping dynamics, see fig. 6.1b. Different regions of initial conditions, which were previously on different sides of a KAM curve (for smaller k), now may become distributed over phase space in a similar

Fig. 6.1 – See also fig. 5.2. Images taken from [1].

(a) KAM curves confine erratic motion introduced by hyperbolic fixed points.



(b) When a KAM curves breaks-up, this erratic motion can spread, although not necessarily.



fashion and loose the correlation with their initial state. This would indicate some form of irreversible behaviour of the physical system. It should be stress that this can now possibly occur but it is not necessarily that such dispersion will occur.

6.2 Moser's Twist Theorem

The preserved surfaces, the KAM curves, are a special subgroup of the $K = 0$ irrational circles, even though they are generally distorted, and so are no longer circles, see figs 5.2 and 5.3. This subgroup is characterised by the fact that their irrational rotation number is not closely approximated by rational numbers m/n with small values of n . Indeed, the specific condition is given by Moser's twist theorem, which states that if the rotation number satisfies the inequality

$$\left| \rho - \frac{m}{n} \right| > \frac{C}{n^{2.5}} \quad (6.1)$$

for some constant $C > 0$ and $m, n \in \mathbb{Z}$, then the surface is preserved for sufficiently small values of $K \neq 0$. All irrational numbers can be approximated to any accuracy by rational numbers m/n provided that n is sufficiently large. The magni-

tude of K which is required to destroy a particular KAM curve apparently depends on “how irrational” the rotation number is associated with that curve. The interesting and important problem is to determine the values of K which destroy the various KAM curves.

6.3 The Break-up of KAM Curves

Let us now consider briefly some methods to determine the value of k which destroys a KAM surface. To show that a KAM curve exists we would have to show that a sequence of mapping of a point on that curve (an orbit) never repeats itself, but rather covers the curve ergodically, so of course, this rules out a numerical approach since we would need to perform an infinite amount of iterations to establish that such a curve exists. Thus we need an alternative approach to the problem.

Greene introduced such an alternative approach which is based on the stability property of certain finite, rational (periodic) trajectories generated by the standard map [2]. He suggested that we should consider a sequence of periodic orbits with rotation numbers, ρ_N , which converge to the irrational rotation number, ρ , of the particular KAM curve of interest. His hypothesis was that when these nearby orbits were “stable”, the circle should exist, and when they were “unstable”, it should be destroyed.

A systematic way to develop a sequence of rational approximations of some ρ is to employ the unique continued fraction representation of the irrational ρ

$$\rho = a_0 + \cfrac{1}{a_1 + \cfrac{1}{a_2 + \dots}} \equiv [a_0, a_1, a_2, \dots] \quad (6.2)$$

where the $a_n \in \mathbb{Z}^+$. So, for example

$$\begin{aligned} e - 1 &= [1, 1, 2, 1, 1, 4, 1, 1, 6, 1, 1, 8, \dots] \\ &= 1.718281828459\dots \end{aligned} \quad (6.3)$$

whereas

$$\frac{(e - 1)}{2} = [0, 1, 6, 10, 14, 18, \dots] \quad (6.4)$$

By truncating the continued fraction at the N th term, we obtain the rational approximation

$$\rho_N = [a_0, a_1, \dots, a_N] \quad (6.5)$$

which is called the N -th convergent of ρ .

The differences $\rho - \rho_0$ alternate in sign as N is increased, so ρ_N converge onto the KAM curve from both sides. To illustrate this, the first five convergents of $e - 1$ are $[1] = 1$, $[1, 1] = 2$, $[1, 1, 2] = 1.666\dots$, $[1, 1, 2, 1] = 1.75$ and $[1, 1, 2, 1, 1] = 1.7143\dots$ whereas the first five convergents of $(e - 1)/2$ are $[0] = 0$, $[0, 1] = 1$, $[0, 1, 6] = 0.85714\dots$, $[0, 1, 6, 10] = 0.859155\dots$ and $[0, 1, 6, 10, 14] = 0.859140859$. However, this also illustrates a second point. Notice that the convergence of the approximations is far faster in the $(e - 1)/2$ case ($|\rho - \rho_5|/\rho \approx 6 \times 10^{-8}$) than in the $e - 1$ case ($|\rho - \rho_5|/\rho \approx 2 \times 10^{-3}$). This is because the values of the a_N 's are much larger for the irrational number $(e - 1)/2$ than they are for $(e - 1)$.

The group of irrational numbers which are most difficult to approximate by rational numbers are those with the continued fraction form $[a_0, a_1, \dots, a_m, 1, 1, \dots]$, i.e. $a_k = 1 \forall k > m$. This forms an equivalence class of irrationals, which Percival called *Noble numbers*. KAM curves with noble rotation numbers appear to be the most robust KAM curves as K increases [2]. The most famous member of this class is

$$\rho^* \equiv [1, 1, 1, \dots] = \frac{(1 + \sqrt{5})}{2} \quad (6.6)$$

which is known as the *golden mean*. The golden mean is most difficult irrational number to approximate with rational numbers. It is, perhaps, not surprising therefore, as noted and established by Greene, that the last KAM curve to be destroyed as K is increased, is the one with the rotation number ρ^* . Interestingly, the rational approximations (eqn. 6.5) of the golden mean are

$$\rho_N^* = 1 + \frac{F_N}{F_{N+1}}$$

where F_N is the N -th Fibonacci number, defined by the recurrence relation $F_{N+1} = F_N + F_{N-1}$ with $F_0 = 0$ and $F_1 = 1$.

We saw earlier that the eigenvalues of a particular fixed point are completely defined by the trace of the Jacobian at that fixed point, see eqn. 3.9. Based on this Greene introduced the residue as

$$R = \frac{1}{4} [2 - \text{tr}(J)] \quad (6.7)$$

According to eqn. 3.9, the perturbations near that fixed point are hyperbolic if $R \geq 0$ or $R \leq 0$, and elliptic if $0 < R < 1$. Greene computed the residues R_N of the orbits ρ_N as $N \rightarrow \infty$ and observed that if $K < K_{cr}(\rho)$, $R_N \rightarrow 0$, and the KAM curve exists. When $K > K_{cr}(\rho)$, $R_N \rightarrow \infty$ and the circle is destroyed. At the critical parameter, i.e. when $K = K_{cr}(\rho)$, R_N remains bounded and the KAM curve exists but appears to be non-smooth. As we can see the value of k that destroys a KAM curve, K_{cr} , depends on the rotation number ρ of the particular KAM curve in question, i.e. $K_{cr}(\rho)$.

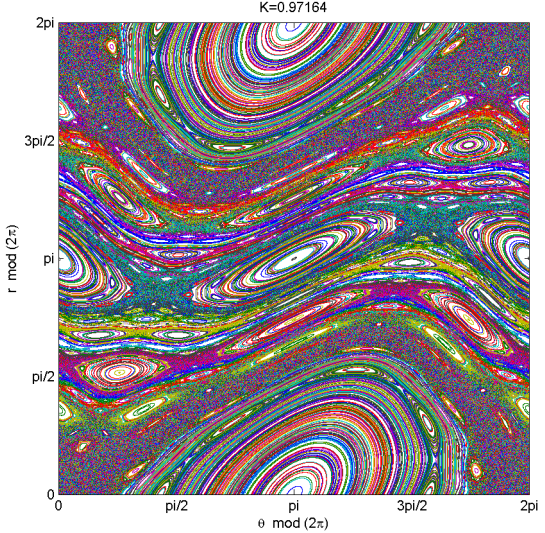
As we already saw above, the magnitude of K which is required to destroy a particular KAM curve apparently depends on “how irrational” the rotation number is associated with that curve. We saw that we can define “how irrational” a particular rotation number is by how easy (or difficult) it is to obtain its rational approximation with eqn. 6.5. Greene found that the KAM curve with its rotation number equal to the golden ratio ρ^* , which is most difficult rational number to approximate with rational numbers, corresponded to the last main KAM curve that existed. The critical value of K , where this curve breaks up, Greene found to be

$$K_{cr}(\rho^*) = 0.971635406\dots \quad (6.8)$$

For reasons discussed above, if $K < K_{cr}(\rho^*)$, the system may exhibit widespread stochastic dynamics throughout the phase plane. It is for this reason that above this value the chaotic regions of the phase space start to dominate the phase space, since now a point has the possibility to freely wander up and down across the phase space of the standard map under iterations, whereas below this value of K it could not do so (this is not to say a given initial condition does wander up and down across the phase space, but merely that it could now do so).

Greene’s method can also be applied to other (non-main) KAM curves and has been done so by by Shenker and Kadanoff [2]. A renormalisation method has been proposed which indicates how every KAM surface breaks up as a function of K [2].

Fig. 6.2 – The standard map for $K = 0.97164$



Part II. Chaotic Control

7 Chaotic Control Theory

7.1 Why are we interested?

Even if we were disregard researching this topic for pure interest, chaotic control theory has many practical applications. Control theory is of great practical importance to many engineering problems, to the point that control theory is regarded as an interdisciplinary branch of engineering and mathematics.

The control of a bouncing ball is a prototype problem for the control of non-linear periodic motions despite the fact that it is arguably one of the simplest physical systems that can yield chaotic dynamics. In fact, the system is so simple that experimental work has be done on this particular control method and system [8].

7.2 What is Chaotic Control?

Small perturbations of a chaotic system can control chaos. Before continuing, we should state exactly what is meant by both chaos and control:

Chaos

- Exponential sensitivity to small changes in initial conditions or any perturbation (the Butterfly Effect)
- Complicated orbital dynamics

Both of these fundamental attributes of chaotic dynamical systems can be taken advantage of to devise chaos control methods

Control

- By control we mean feedback control: measurements of the current state of the system are taken, and, on the basis of these measurements, some *controllable parameter* (or set of parameters) is adjusted so as to achieve the desired goal
- By control we mean optimal control

The goals of different chaotic control system can be varied. For example, one might stabilise an unstable periodic orbit; or perhaps one might direct

chaotic trajectories to desired locations. However, these are not the only possible goals.

8 Controlling a Bouncing Ball

8.1 High Ball Map under Frequency Control

The focus of this section is to develop an algorithm which will control the bouncing ball. Our goal is to maintain the system at a specified fixed point of our map that, without control, would be unstable. *We want to use the plate frequency as the control parameter.*

Recall the high bounce map, eqns. 8.1

$$\dot{y}_{j+1} = -a_2 \dot{y}_j + a_1 A \bar{\omega} \cos(\theta_{j+1}) \quad (8.1a)$$

$$\theta_{j+1} = \theta_j + \bar{\omega} \left(\frac{2\dot{y}_j}{g} \right) \bmod 2\pi \quad (8.1b)$$

where we have dropped the “+” superscript, as it is superfluous here, and we have changed the ω that was in the original eqns. to an $\bar{\omega}$ for notational clarity.

The plate frequency just after a bounce at time t_j is given by

$$\omega_j = \bar{\omega} + u_j \quad (8.2)$$

where u_j is the change in frequency from the nominal frequency. Hence,

$$\dot{y}_{j+1} = -a_2 \dot{y}_j + a_1 A \omega_j \cos(\theta_{j+1}) \quad (8.3a)$$

$$\theta_{j+1} = \theta_j + \omega_j \left(\frac{2\dot{y}_j}{g} \right) \bmod 2\pi \quad (8.3b)$$

is the high bounce map with control. However, it is not yet in its most compact form. Multiply eqn. 8.3a through by $2\bar{\omega}/g$ yielding

$$\frac{2\bar{\omega}}{g} \dot{y}_{j+1} = -a_2 \frac{2\bar{\omega}}{g} \dot{y}_j + a_1 \frac{2\bar{\omega}}{g} A \omega_j \cos(\theta_{j+1}) \quad (8.4a)$$

$$\theta_{j+1} = \theta_j + \omega_j \left(\frac{2\dot{y}_j}{g} \right) \bmod 2\pi \quad (8.4b)$$

We now preform a rescaling by setting

$$\psi_j \equiv \frac{2\bar{\omega}}{g} \dot{y}_j \quad \text{and} \quad \hat{a}_1 \equiv \frac{2a_1}{g} A$$

and we also, for the sake of notational clarity, define $\phi_j \equiv \theta_j$. This yields

Hence,

$$\psi_{j+1} = -a_2\psi_j + \hat{a}_1\bar{\omega}\omega_j \cos(\phi_{j+1}) \quad (8.5a)$$

$$\phi_{j+1} = \phi_j + \frac{\omega_j}{\bar{\omega}}\psi_j \mod 2\pi \quad (8.5b)$$

which is the *high bounce map with control* in the desired form.

We now have a choice for the value of the control parameter ω_j : with this choice, we could select any value we desired for ψ_{j+1} ; or, we could select any value we desired for ϕ_{j+1} . We cannot, however, select any value we desired for ψ_{j+1} while simultaneously selecting any value we desire for ϕ_{j+1} . Rather, the values of ψ_{j+1} and ϕ_{j+1} are both determined by a particular choice of ω_j . However, in the region of a fixed point we can chose a value of ω_j such that the next iterate is closer to the fixed point. We seek a feedback control method, that is a method for selecting the ω_j 's, that will do just this.

8.2 Optimal Control

However, as we have already stated, we want optimal control. That is, we don't just want to approach the mixed point; we want to approach the unstable fixed point in the most efficient manner possible. In this case, the control parameter is the frequency ω_j . We obtained this value by changing the nominal frequency $\bar{\omega}$ by and amount u_j . So, optimal control in this method involves minimising the changes in the nominal frequency, i.e. minimising the u_j 's. The approach taken in the design of this feedback controller is to assume that the system is close enough to the fixed point so that a linear approximation is a valid approximation of the map

8.3 Fixed Points

We seek an unstable fixed point of the map when no control is applied, i.e. when $u_j = 0$ and so $\omega_j = \bar{\omega}$. Thus, we seek solutions to

$$\bar{\psi} = -a_2\bar{\psi} + \hat{a}_1\bar{\omega}^2 \cos(\bar{\phi} + \bar{\psi}) \quad (8.6a)$$

$$\bar{\phi} = \bar{\phi} + \bar{\psi} \mod 2\pi \quad (8.6b)$$

$$(1 + a_2)\bar{\psi} = \hat{a}_1\bar{\omega}^2 \cos(\bar{\phi} + \bar{\psi}) \quad (8.7a)$$

$$0 = \bar{\psi} \mod 2\pi \quad (8.7b)$$

$$\bar{\phi} = \cos^{-1} \left(\frac{2\pi n(1 + a_2)}{\hat{a}_1\bar{\omega}^2} \right) \quad (8.8a)$$

$$\bar{\psi} = 2\pi n \quad (8.8b)$$

8.4 Linearisation

Define the displacement from the unstable fixed point

$$x_1 = \phi - \bar{\phi} \quad (8.9a)$$

$$x_2 = \psi - \bar{\psi} \quad (8.9b)$$

and we also have that

$$u = \omega - \bar{\omega} \quad (8.9c)$$

From eqn. 8.5b we have that

$$\begin{aligned} x_{1_{j+1}} + \bar{\phi} &= x_{1_j} + \bar{\phi} + \frac{u_j + \bar{\omega}}{\bar{\omega}} (x_{2_j} + \bar{\psi}) \\ x_{1_{j+1}} &= x_{1_j} + 2\pi \frac{u_j}{\bar{\omega}} + x_{2_j} + 2\pi \\ &= x_{1_j} + x_{2_j} + \frac{\bar{\psi}}{\bar{\omega}} u_j \end{aligned} \quad (8.10a)$$

where we have dropped non-linear terms.

From eqn. 8.4a we have that

$$\begin{aligned} x_{2_{j+1}} + \bar{\psi} &= -a_2 x_{2_j} - a_2 \bar{\psi} \dots \\ &\dots + \hat{a}_1 \bar{\omega} (u_j + \bar{\omega}) \cos(x_{1_{j+1}} + \bar{\phi}) \end{aligned}$$

now, from eqns. 8.7a and 8.8b we have that

$$(1 + a_2)\bar{\psi} = \hat{a}_1\bar{\omega}^2 \cos \bar{\phi}$$

and hence

$$\begin{aligned} x_{2_{j+1}} + \hat{a}_1\bar{\omega}^2 \cos \bar{\phi} &= -a_2 x_{2_j} \dots \\ &\dots + \hat{a}_1\bar{\omega}^2 \cos(x_{1_{j+1}} + \bar{\phi}) \dots \\ &\dots + \hat{a}_1\bar{\omega} u_j \cos(x_{1_{j+1}} + \bar{\phi}) \end{aligned}$$

Taking a series expansion of the last two terms and dropping non-linear terms we get

$$\begin{aligned} x_{2_{j+1}} + \hat{a}_1\bar{\omega}^2 \cos \bar{\phi} &= -a_2 x_{2_j} \dots \\ &\dots + \hat{a}_1\bar{\omega}^2 \cos \bar{\phi} - \hat{a}_1\bar{\omega}^2 x_{1_{j+1}} \sin \bar{\phi} \dots \\ &\dots + \hat{a}_1\bar{\omega} u_j \cos \bar{\phi} \end{aligned}$$

and by inserting eqn. 8.10a we obtain

$$\begin{aligned} x_{2j+1} &= -a_2 x_{2j} \dots \\ &\dots - \hat{a}_1 \bar{\omega}^2 \sin \bar{\phi} \left(x_{1j} + x_{2j} + \frac{\psi}{\bar{\omega}} u_j \right) \dots \\ &\dots + \hat{a}_1 \bar{\omega} u_j \cos \bar{\phi} \end{aligned}$$

$$\begin{aligned} x_{2j+1} &= -a_2 x_{2j} - \hat{a}_1 \bar{\omega}^2 x_{1j} \sin \bar{\phi} \dots \\ &\dots - \hat{a}_1 \bar{\omega} \psi u_j \sin \bar{\phi} - \hat{a}_1 \bar{\omega}^2 x_{2j} \sin \bar{\phi} \dots \\ &\dots + \hat{a}_1 \bar{\omega} u_j \cos \bar{\phi} \quad (8.10b) \end{aligned}$$

Hence, from eqns. 8.10a and 8.10b we see that our linear map is given by

$$\underline{x}_{j+1} = \underline{A}\underline{x}_j + \underline{B}u_j \quad (8.11)$$

where

$$\begin{aligned} \underline{x}_j &= \begin{pmatrix} x_1 \\ x_2 \end{pmatrix} \\ \underline{A} &= \begin{pmatrix} 1 & 1 \\ a_{21} & -a_2 + a_{21} \end{pmatrix} \end{aligned}$$

and

$$\underline{B} = \begin{pmatrix} \frac{\psi}{\bar{\omega}} \\ a_{21} \frac{\bar{\omega}}{\bar{\omega}} + \hat{a}_1 \bar{\omega} \cos \bar{\phi} \end{pmatrix}$$

where $a_{21} = -\hat{a}_1 \bar{\omega}^2 \sin \bar{\phi}$.

8.5 LQR Method

Given a system of the form of eqn. 8.11 we have two possibilities:

- Minimise

$$\sum_{i=k}^{\infty} \underline{x}_i \cdot Q \underline{x}_i$$

as a way to select the best possible control, i.e. to select the control that produces the overall smallest transient displacement as our iterates approach the fixed point.

- Minimise

$$\sum_{i=k}^{\infty} u_i R u_i$$

The matrix Q must be positive definite while the scalar R must be positive. The matrix Q allows one to preferentially select which of the two state variables is more important to control, while the

value of R relative to the values in Q allow one to select between better control or better efficiency.

The linear-quadratic regulator is a control design method used to design controllers for systems in the form of eqn. 8.11. The LQR method is more general than this however, and the control input can be a vector of control parameters. We only require the scalar input as we only have one control parameter (u_j 's).

Theorem. Let

$$J = \sum_{i=k}^{\infty} [\underline{x}_i \cdot Q \underline{x}_i + u_i \cdot R u_i]$$

Then the optimal control is given by the state feedback law

$$u_i = -K \underline{x}_i$$

where

$$K = (R + B^T P B)^{-1} B^T P A$$

and where P is the solution to the discrete time algebraic Riccati equation

$$A^T P A - P - A^T P B (R + B^T P B)^{-1} B^T P A + Q = 0$$

Proof of this theorem can be found in sec. 10. Thus, to find the LQR feedback gain matrix K

- Select the design matrices Q and R
- Solve the discrete time algebraic Riccati equation for P
- Find $K = (R + B^T P B)^{-1} B^T P A$

This process can be carried out in MATLAB using the `d1qr(A, B, Q, R)` function. Once the gain matrix K has been calculated we can calculate the change in frequency we need to apply from

$$\begin{aligned} u_j &= -K \underline{x}_j \\ &= -k_1 x_{1j} - k_2 x_{2j} \\ &= -k_1 (\phi_j - \bar{\phi}) - k_2 (\psi_j - \psi) \quad (8.12) \end{aligned}$$

Hence,

$$\omega_j = \bar{\omega} - k_1 (\phi_j - \bar{\phi}) - k_2 (\psi_j - \psi) \quad (8.13)$$

So, the optimal controlled high bounce map is given by eqns. 8.5 and eqn. 8.13, i.e.

$$\omega_j = \bar{\omega} - k_1 (\phi_j - \bar{\phi}) - k_2 (\psi_j - \psi) \quad (8.14a)$$

$$\psi_{j+1} = -a_2 \psi_j + \hat{a}_1 \bar{\omega} \omega_j \cos(\phi_{j+1}) \quad (8.14b)$$

$$\phi_{j+1} = \phi_j + \frac{\omega_j}{\bar{\omega}} \psi_j \mod 2\pi \quad (8.14c)$$

8.6 Ball under Control

Note: in this section the calculations were done using the MATLAB code found in sec. 11.7.1.

The following values were used for the constant parameters of our system

$$\begin{aligned}\hat{a}_1 &= 0.004594 \\ a_2 &= -0.733333\end{aligned}$$

Now, taking $\bar{\omega} = 30$ we calculate the $n = 1$ fixed point from eqns. 8.8

$$\begin{aligned}\bar{\psi} &= 2\pi \\ \bar{\phi} &= 1.1536\end{aligned}$$

Linearisation around this fixed point yields

$$A = \begin{pmatrix} 1 & 1 \\ -3.7799 & -3.0466 \end{pmatrix}$$

and

$$B = \begin{pmatrix} 0.2094 \\ -0.7358 \end{pmatrix}$$

The eigenvalues of the system without control, i.e. the eigenvalues of A are

$$\begin{aligned}\lambda_1 &= -1.5834 \\ \lambda_2 &= 0.4631\end{aligned}$$

thus it is indeed a hyperbolic fixed point.

Using LQR control design with $Q = \mathbb{I}_2$ and $R = 1$, the `dlqr(A, B, Q, R)` function returns

$$K = \begin{pmatrix} 3.9309 \\ 2.8428 \end{pmatrix}$$

The eigenvalues of the controlled system $C = A - BK$ are

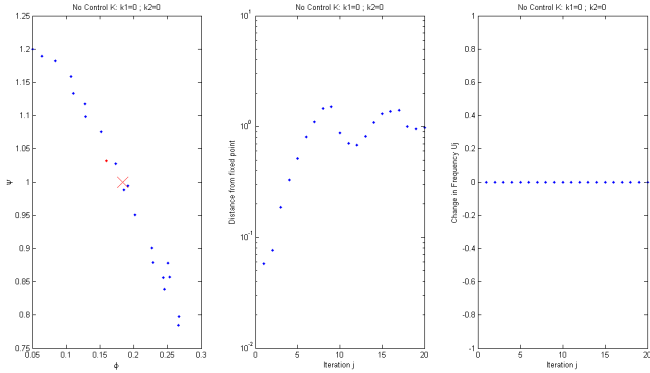
$$\begin{aligned}\lambda_1 &= -0.3890 + 0.1975i \\ \lambda_2 &= -0.3890 - 0.1975i\end{aligned}$$

Thus, we can see that our system is now a stable at what was an unstable fixed point.

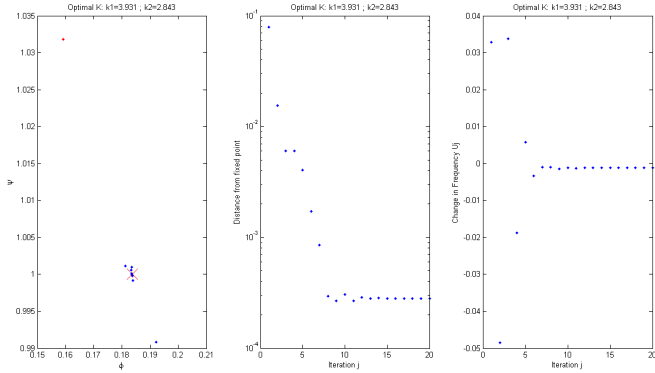
Figs. 8.1 show an example of the result of the above consideration for a particular initial condition.

Fig. 8.1 – Control of the bouncing ball: the following plot so the ball map with: no control; optimal control; and non-optimal control. The red \times is the location of the unstable, hyperbolic fixed point (without control). The red \cdot shows the initial condition while the blue \cdot show the locations of subsequent iterates. See sec. 11.7.2 for the MATLAB script used to create this plot.

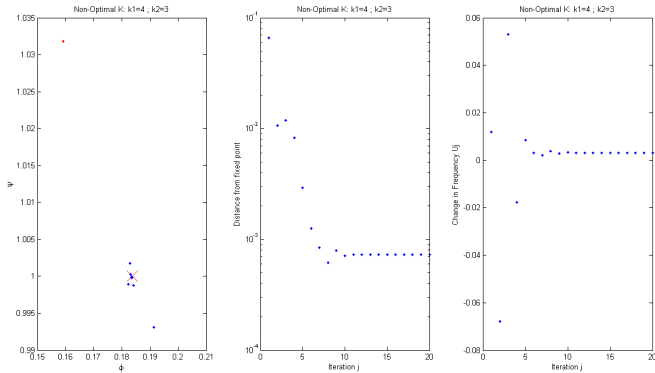
(a) The bouncing ball with no control applied.



(b) The bouncing ball with optimal control applied.



(c) The bouncing ball with non-optimal control applied. Notice that the changes in frequency u_j are larger than in the optimal control case.



Part III. Appendices

9 Area-Preserving Twist Maps

The standard map is a particular example of the general twist map

$$r_{n+1} = r_n + \varepsilon\alpha(r_n, \theta_n) \quad (9.1a)$$

$$\theta_{n+1} = \theta_n + 2\pi\rho(r_n) + \varepsilon\beta(r_n, \theta_n) \quad (9.1b)$$

where $\rho(r)$ is the rotation number if $\varepsilon = 0$. The functions $\alpha(r, \theta)$, $\beta(r, \theta)$ and $\rho(r)$ satisfy the area preserving condition (the Jacobian of the map must equal 1) and $\alpha(r, \theta + 2\pi) = \alpha(r, \theta)$ and $\beta(r, \theta + 2\pi) = \beta(r, \theta)$. The map has the same properties as the standard map provided that $\varepsilon \approx 0$

10 Discrete Time LQR

Given the discrete-time system

$$x_{k+1} = Ax_k + Bu_k \quad (10.1)$$

we want a state-variable feedback control

$$u_k = -Kx_k \quad (10.2)$$

that minimises the cost function

$$J(x_k) = \sum_{i=k}^{\infty} [x_i \cdot Qx_i + u_i \cdot Ru_i] \quad (10.3)$$

Assuming that the design matrices

$$Q = Q^T \geq 0$$

$$R = R^T > 0$$

Theorem. Let

$$J = \sum_{i=k}^{\infty} [x_i \cdot Qx_i + u_i \cdot Ru_i]$$

Then the optimal control is given by the state feedback law

$$u_i = -Kx_i$$

where

$$K = (R + B^T PB)^{-1} B^T PA$$

and where P is the solution to the discrete algebraic Riccati equation

$$A^T PA - P - A^T PB (R + B^T PB)^{-1} B^T PA + Q = 0$$

Proof. Substitute eqn. 10.2 into eqn. 10.3

$$J(x_k) = \sum_{i=k}^{\infty} [x_i \cdot (Q + K \cdot RK) x_i] \quad (10.4)$$

Eqn. 10.1 becomes

$$x_{k+1} = (A - BK) x_k = A, \quad (10.5)$$

Rewrite eqn. 10.3

$$J(x_k) = (x_k \cdot Qx_k + u_k \cdot Ru_k) + J(x_{k+1}) \quad (10.6)$$

Assume that the optimal cost is given for all k in the form

$$J^*(x_k) = x_k \cdot Px_k \quad (10.7)$$

where P is an unknown kernel.

Substitute eqn. 10.7 into eqn. 10.6

$$J = x_k \cdot Px_k = \frac{1}{2} (x_k \cdot Qx_k + u_k \cdot Ru_k) + x_{k+1} \cdot Px_{k+1} \quad (10.8)$$

Using eqn. 10.1

$$J = \frac{1}{2} (x_k \cdot Qx_k + u_k \cdot Ru_k) + (Ax_k + Bu_k) \cdot P (Ax_k + Bu_k) \quad (10.9)$$

Minimise J with respect to u_k

$$\frac{\partial J}{\partial u_k} = \frac{1}{2} \frac{\partial}{\partial u_k} (u_k \cdot Ru) + \frac{\partial}{\partial u_k} \{(Bu_k) \cdot PAx_k + (Ax_k) \cdot PBu_k + (Bu_k) \cdot PBu_k\} = 0 \quad (10.10)$$

$$\frac{\partial}{\partial u_k} (u_k \cdot Ru_k) = 2u_k^T R^T$$

$$\frac{\partial}{\partial u_k} \{(Bu_k) \cdot PAx_k\} = \frac{\partial}{\partial u_k} (u_k B^T PAx_k) = x_k^T (B^T PA)^T$$

$$\frac{\partial}{\partial u_k} \{(Ax_k) \cdot PBu_k\} = (Ax_k)^T PB$$

$$\frac{\partial}{\partial u_k} \{(Bu_k) \cdot PBu_k\} = \frac{\partial}{\partial u_k} (u_k^T B^T PBu_k) = 2u_k^T B^T PB$$

Eqn. 10.10 \implies

$$\begin{aligned} 0 &= 2u_k^T R^T + 2u_k^T B^T PB + 2x_k^T A^T P^T B \\ &= u_k^T (R^T + B^T PB) + x_k^T A^T P^T B \end{aligned}$$

Taking the transpose we get the optimal control as

$$(R + B^T PB) u_k = -B^T PAx_k$$

or

$$u_k = -(R + B^T PB)^{-1} B^T PAx_k$$

Hence, the optimal gain is then

$$K = (R + B^T PB)^{-1} B^T PA \quad (10.11)$$

To find P , put $u_k = -Kx_k$ into eqn. 10.9.

$$x_k^T [-P + Q + K^T RK + A^T PA + A^T PBK - K^T B^T PA + K^T B^T PBK] x_k = 0$$

or, rearranging

$$x_k^T [-P + Q + K^T RK + (A - BK)^T P (A - BK)] x_k = 0 \quad (10.12)$$

This must hold for all x_k 's and therefore

$$-P + Q + K^T RK + (A - BK)^T P (A - BK) = 0 \quad (10.13)$$

Now, K was given by eqn. 10.11

$$\begin{aligned} 0 &= \left[A - B (R + B^T PB)^{-1} B^T PA \right]^T P \left[A - B (R + B^T PB)^{-1} B^T PA \right] \dots \\ &\dots - P + Q + \left[(R + B^T PB)^{-1} B^T PA \right]^T R \left[(R + B^T PB)^{-1} B^T PA \right] \end{aligned} \quad (10.14)$$

Which, can be rewritten as

$$0 = A^T PA - P + Q - A^T PB (R + B^T PB)^{-1} B^T PA - (BK)^T P (A - BK) + K^T RK \quad (10.15)$$

But, the second line of eqn. 10.15 can be shown to be 0

$$\begin{aligned} -(BK)^T P (A - BK) + K^T RK &= K^T [B^T P (A - BK) - RK] \\ &= K^T [B^T PA - B^T PBK - RK] \\ &= K^T [B^T PA - (B^T PB + R) K] \end{aligned}$$

But, K was given by eqn. 10.11

$$K^T [B^T PA - (B^T PB + R) (B^T PB + R)^{-1} B^T PA] = 0$$

Therefore, eqn. 10.14 indeed reduces to

$$0 = A^T PA - P + Q - A^T PB (R + B^T PB)^{-1} B^T PA \quad (10.16)$$

which is the discrete time algebraic Riccati equation. \square

11 MATLAB Scripts

11.1 M-Files for Fig. 2.1 and figs. 2.2

```

1 clear all;
2
3 % This can be changed to select the required K value
4 k=0.8;
5
6 for n=1:10
7
```

```

8 p(1,n)=rand;
9 q(1,n)=rand;
10
11 for i=2:5000
12     % We can add in some phase shifts here to focus the plot
13     % on were we want
14     p(i,n)=mod((p(i-1,n)-((k/(2*pi))*sin(2*pi*q(i-1,n)))),1);
15     q(i,n)=mod((q(i-1,n)+p(i,n)+0.5),1);
16 end
17 end
18
19 scrsz=get(0,'ScreenSize')
20 set(0,'DefaultFigurePosition',[scrsz(1) scrsz(2) scrsz(3) scrsz(4)]);
21
22 plot(q,p,'.', 'MarkerSize',1)
23
24 axis([0 1 0 1])
25 box on
26 title(['K=',num2str(k)]);
27 set(gca,'XTick',0:0.25:1)
28 set(gca,'YTick',0:0.25:1)
29 set(gca,'XTickLabel',{'0','pi/2','pi','3pi/2','2pi'})
30 set(gca,'YTickLabel',{'0','pi/2','pi','3pi/2','2pi'})
31 xlabel('{\theta} mod (2\pi)');
32 ylabel('r mod (2\pi)');
33 axis square
34
35 saveas(gcf, ['iter-37.png'])

```

11.2 M-Files for Figs. 2.3

11.2.1 M-File for Fig. 2.3 (a)

```

1 clear all;
2
3 k=0.5;
4
5 h(1)=pi;
6
7 figure('PaperSize',[400 400])
8 polar(0,10)
9 hold on;
10
11 for n=[0.18,0.4,0.86]
12
13     p(1)=2*pi*n;
14     for i=2:1000
15         h(i)=h(i-1)+p(i-1);
16         p(i)=p(i-1)+(k*sin(h(i)));
17     end
18     polar(h,p,'.')
19     hold all;
20 end
21
22 title('(a)', 'FontSize', 20);

```

11.2.2 M-File for Fig. 2.3 (b)

```

1 clear all;
2
3 k=0.5;
4
5 q(1)=0.5;
6
7 for n=[0.18,0.4,0.86]
8
9     p(1)=n;
10    for i=2:1000
11        p(i)=mod(p(i-1)-((k/(2*pi))*sin(2*pi*q(i-1)+pi)),1);
12        q(i)=mod((q(i-1)+p(i)),1);
13    end
14    plot(q,p,'.')
15    hold all;
16 end
17
18 xlabel('q mod(1)');
19 ylabel('p mod(1)');
20
21 title('(b)', 'FontSize', 20);

```

11.2.3 M-File for Fig. 2.3 (c)

```

1 clear all;
2
3 k=0.5;
4
5 q=0.5;
6
7 for n=[0.18,0.4,0.86]
8
9     p(1)=n;
10    for i=2:1000
11        p(i)=p(i-1)-((k/(2*pi))*sin(2*pi*q(i-1)+pi));
12        q(i)=mod((q(i-1)+p(i)),1);
13    end
14    plot(q,p,'.')
15    hold all;
16 end
17
18 xlabel('q mod(1)');
19 ylabel('p');
20
21 title('(c)', 'FontSize', 20);

```

11.3 M-File for Fig. 3.1

```

1 clear all;
2
3 k=0;
4
5 h(1)=pi;
6
7 polar(0,3)

```

```

8 hold on;
9
10 p(1)=2*pi*(1/(2*sqrt(2)));
11 h(1)=pi;
12
13 for i=2:1000
14     h(i)=h(i-1)+p(i-1);
15     p(i)=p(i-1)+(k*sin(h(i)));
16 end
17 h = polar(h,p,'r.');
18
19 clear p;
20 clear h;
21
22 p(1)=2*pi*(1/8);
23 h(1)=pi;
24
25 for i=2:1000
26     h(i)=h(i-1)+p(i-1);
27     p(i)=p(i-1)+(k*sin(h(i)));
28 end
29 h = polar(h,p,'b.');

```

11.4 M-File for Fig. 3.1

```

1 clear all;
2
3 k=0.0001;
4
5 h(1)=pi;
6
7 polar(0,1)
8 hold on;
9
10 p(1)=2*pi*(1/7.9);
11 h(1)=pi;
12
13 for i=2:32
14     h(i)=h(i-1)+p(i-1);
15     p(i)=p(i-1)+(k*sin(h(i)));
16 end
17 h = polar(h,p,'r.');
18 set( findobj(h), 'MarkerSize', 5 );
19
20
21 p(1)=2*pi*(1/8);
22 h(1)=pi;
23
24 for i=2:32
25     h(i)=h(i-1)+p(i-1);
26     p(i)=p(i-1)+(k*sin(h(i)));
27 end
28 h = polar(h,p,'k.');
29 set( findobj(h), 'MarkerSize', 10 );
30
31
32 p(1)=2*pi*(1/8.1);
33 h(1)=pi;
34

```

```

35
36 for i=2:32
37     h(i)=h(i-1)+p(i-1);
38     p(i)=p(i-1)+(k*sin(h(i)));
39 end
40 h = polar(h,p,'b.');
41 set( findobj(h), 'MarkerSize',5);

```

11.5 M-File for Figs. 4.6

```

1 clear all;
2
3 k=0.971635;
4
5 iter=18;
6
7 J=[1,1;k,(1+k)];
8 x=eig(J);
9 if x(1)<x(2)
10     lambda=x(1);
11 else
12     lambda=x(2);
13 end
14 lambda
15
16 dq=0.000005;
17
18 q=(0.001/2*pi):(dq/2*pi):(0.005/2*pi);
19 p=(1-lambda)*q;
20 q(:)=q(:)+0.5;
21 p(:)=p(:)+0.5;
22
23 dp=p(2)-p(1);
24
25 n=length(p);
26
27 for j=1:n
28     q(j,1)=q(j);
29     p(j,1)=p(j);
30 end
31
32 for j=2:iter
33     for i=1:n
34         p(j,i)=mod((p(j-1,i)-((k/(2*pi))*sin(2*pi*q(j-1,i)))),1);
35         q(j,i)=mod((q(j-1,i)+p(j,i)+0.5),1);
36     end
37 end
38
39 figure(1)
40 for j=1:6
41     subplot(3,2,j)
42     plot(q(j,:),p(j,:),'.', 'markersize',1)
43     title(['Mapping applied ', num2str(j-1), ' times']);
44     xlabel('(\theta) mod(1)');
45     ylabel('r mod(1)');
46     axis([0 1 0 1])
47     hold on;
48 %     pause(1);
49 end

```

```

50
51 figure(2)
52 for j=7:12
53 subplot(3,2,j-6)
54 plot(q(j,:),p(j,:),'.', 'markersize',1)
55 title(['Mapping applied ',num2str(j-1), ' times']);
56 xlabel('{\theta} mod(1)');
57 ylabel('r mod(1)');
58 axis([0 1 0 1])
59 hold on;
60 % pause(1);
61 end
62
63 figure(3)
64 for j=13:iter
65 subplot(3,2,j-12)
66 plot(q(j,:),p(j,:),'.', 'markersize',1)
67 title(['Mapping applied ',num2str(j-1), ' times']);
68 xlabel('{\theta} mod(1)');
69 ylabel('r mod(1)');
70 axis([0 1 0 1])
71 hold on;
72 % pause(1);
73 end

```

11.6 M-File for Figs. 5.5

```

1 clear all;
2 kvals=[0,0.02,0.25,0.6,0.75,0.85];
3
4 figure(1)
5 for j=1:3
6
7 k=kvals(j);
8
9 for n=1:8
10
11 p(1,n)=0.97-0.12*(n-1);
12 q(1,n)=0.49;
13
14 for i=2:10000
15 p(i,n)=mod((p(i-1,n)-((k/(2*pi))*sin(2*pi*q(i-1,n)+pi))),1);
16 q(i,n)=mod((q(i-1,n)+p(i,n)),1);
17 end
18 end
19
20 subplot(3,1,j)
21 set(gca, 'ColorOrder', [0 0 1; 0 0.5 0; 1 0 0; 0 0.75 0.75;...
22 0.75 0 0.75; 0.75 0.25 0; 0.25 0.25 0.25; 1 0.4 0.6]...
23 , 'NextPlot','ReplaceChildren')
24 plot(q,p,'.', 'MarkerSize',1)
25 axis square
26 box on
27 title(['K=',num2str(k)]);
28 xlabel('{\theta} mod(1)');
29 ylabel('r mod(1)');
30
31 end
32

```

```

33 figure(2)
34 for j=4:6
35
36 k=kvals(j);
37
38 for n=1:8
39
40 p(1,n)=0.97-0.12*(n-1);
41 q(1,n)=0.49;
42
43 for i=2:10000
44 p(i,n)=mod((p(i-1,n)-((k/(2*pi))*sin(2*pi*q(i-1,n)+pi))),1);
45 q(i,n)=mod((q(i-1,n)+p(i,n)),1);
46 end
47 end
48
49 subplot(3,1,j-3)
50 set(gca, 'ColorOrder', [0 0 1; 0 0.5 0; 1 0 0; 0 0.75 0.75; ...
51 0.75 0 0.75; 0.75 0.25 0; 0.25 0.25 0.25; 1 0.4 0.6]...
52 , 'NextPlot', 'ReplaceChildren')
53 plot(q,p,'.', 'MarkerSize', 1)
54 axis square
55 box on
56 title(['K=' num2str(k)]);
57 xlabel('{\theta} mod(1)');
58 ylabel('r mod(1)');
59
60 end

```

11.7 M-Files for Sec. 8.6

11.7.1 M-File for Linearisation

```

1 clear all
2
3 a1h=0.004594;
4 a2=-0.733333;
5
6 n=1;
7
8 omegabar=30;
9
10 scibar=2*pi*n
11 phibar=acos((2*pi*n*(1+a2))/(a1h*(omegabar^2)))
12
13 a21=-a1h*omegabar^2*sin(phibar);
14
15 A=[1,1; a21,-a2+a21]
16
17 evals=eig(A)
18
19 B=[scibar/omegabar ; a21*scibar/omegabar + a1h*omegabar*cos(phibar) ]
20
21
22 Q=[1,0 ; 0,1];
23 R=1;
24
25 K=dlqr(A,B,Q,R)
26

```

```

27 C=A-B*K
28
29 evalscontrol=eig(C)

```

11.7.2 M-File for Figs. 8.1

```

1 clear all
2
3 p=2*pi+0.2;
4 h=1.0;
5
6 subplot(1,3,1)
7 plot(1.154/(2*pi),2*pi/(2*pi), 'xr', 'markersize', 20)
8 hold on;
9
10 plot(h/(2*pi),p/(2*pi), '.r')
11
12 wbar=30;
13
14
15 hbar=1.153;
16 pbar=2*pi;
17
18 k1=3.931;
19 k2=2.843;
20
21 a1=0.00459;
22 a2=-0.73333;
23
24 scrsz = get(0,'ScreenSize')
25 set(0,'DefaultFigurePosition', [scrsz(1) scrsz(2) scrsz(3) scrsz(4)]);
26
27 figure(1)
28
29 for i=1:20
30     w=wbar-k1*(h-hbar)-k2*(p-pbar);
31     h=mod((h+(w/wbar)*p),(2*pi));
32     p=(-a2*p+(a1*wbar*w*cos(h)));
33     dis(i)=sqrt((h-hbar)^2+(p-pbar)^2);
34     cost=w-wbar;
35     subplot(1,3,1)
36     plot(h/(2*pi),p/(2*pi), '.')
37     hold on;
38     subplot(1,3,3)
39     plot(i,cost, '.')
40     hold on;
41 end
42
43 subplot(1,3,2)
44 semilogy(dis,'.')
45
46 subplot(1,3,1)
47 xlabel('{\phi}');
48 ylabel('{\psi}');
49 title(['Optimal K: k1=',num2str(k1), ' ; k2=',num2str(k2)]);
50
51 subplot(1,3,2)
52 xlabel('Iteration j');
53 ylabel('Distance from fixed point');

```

```

54 title(['Optimal K: k1=',num2str(k1), ' ; k2=',num2str(k2)]);
55
56 subplot(1,3,3)
57 xlabel('Iteration j');
58 ylabel('Change in Frequency Uj');
59 title(['Optimal K: k1=',num2str(k1), ' ; k2=',num2str(k2)]);
60
61 figure(2)
62 p=2*pi+0.2;
63 h=1.0;
64
65 subplot(1,3,1)
66 plot(1.154/(2*pi),2*pi/(2*pi),'xr','markersize',20)
67 hold on;
68
69 plot(h/(2*pi),p/(2*pi),'.r')
70
71 wbar=30;
72
73
74 hbar=1.153;
75 pbar=2*pi;
76
77 k1=4;
78 k2=3;
79
80 a1=0.00459;
81 a2=-0.733;
82
83
84 for i=1:20
85     w=wbar-k1*(h-hbar)-k2*(p-pbar);
86     h=mod((h+(w/wbar)*p),(2*pi));
87     p=(-a2*p+(a1*wbar*w*cos(h)));
88     dis(i)=sqrt((h-hbar)^2+(p-pbar)^2);
89     cost=w-wbar;
90     subplot(1,3,1)
91     plot(h/(2*pi),p/(2*pi),'.')
92     subplot(1,3,3)
93     plot(i,cost,'.')
94     hold on;
95 end
96
97 subplot(1,3,2)
98 semilogy(dis,'.')
99
100 subplot(1,3,2)
101 semilogy(dis,'.')
102
103 subplot(1,3,1)
104 xlabel('{\phi}');
105 ylabel('{\psi}');
106 title(['Non-Optimal K: k1=',num2str(k1), ' ; k2=',num2str(k2)]);
107
108 subplot(1,3,2)
109 xlabel('Iteration j');
110 ylabel('Distance from fixed point');
111 title(['Non-Optimal K: k1=',num2str(k1), ' ; k2=',num2str(k2)]);
112
113 subplot(1,3,3)
114 xlabel('Iteration j');
115 title(['Non-Optimal K: k1=',num2str(k1), ' ; k2=',num2str(k2)]);

```

```

116 ylabel('Change in Frequency Uj');
117
118 figure(3)
119 p=2*pi+0.2;
120 h=1.0;
121
122 subplot(1,3,1)
123 plot(1.154/(2*pi),2*pi/(2*pi),'xr','markersize',20)
124 hold on;
125
126 plot(h/(2*pi),p/(2*pi),'.r')
127
128 wbar=30;
129
130
131 hbar=1.153;
132 pbar=2*pi;
133
134 k1=0;
135 k2=0;
136
137 a1=0.00459;
138 a2=-0.733;
139
140
141 for i=1:20
142     w=wbar-k1*(h-hbar)-k2*(p-pbar);
143     h=mod((h+(w/wbar)*p),(2*pi));
144     p=(-a2*p+(a1*wbar*w*cos(h)));
145     dis(i)=sqrt((h-hbar)^2+(p-pbar)^2);
146     cost=w-wbar;
147     subplot(1,3,1)
148     plot(h/(2*pi),p/(2*pi),'.')
149     subplot(1,3,3)
150     plot(i,cost,'.')
151     hold on;
152 end
153
154 subplot(1,3,2)
155 semilogy(dis,'.')
156
157 subplot(1,3,2)
158 semilogy(dis,'.')
159
160 subplot(1,3,1)
161 xlabel('{\phi}');
162 ylabel('{\psi}');
163 title(['No Control K: k1=',num2str(k1),'; k2=',num2str(k2)]);
164
165 subplot(1,3,2)
166 xlabel('Iteration j');
167 ylabel('Distance from fixed point');
168 title(['No Control K: k1=',num2str(k1),'; k2=',num2str(k2)]);
169
170 subplot(1,3,3)
171 xlabel('Iteration j');
172 title(['No Control K: k1=',num2str(k1),'; k2=',num2str(k2)]);
173 ylabel('Change in Frequency Uj');

```

References

- [1] E. Atlee Jackson, *Perspectives of nonlinear dynamics*, Cambridge University Press, 1990, ISBN978-0-521-42633-5
- [2] Ibid - references therein.
- [3] <http://amath.colorado.edu/faculty/jdm/stdmap.html>
- [4] D. Hobson, *An efficient method for computing invariant manifolds of planar maps*, J. Comput. Phys., 104(1):14-22, 1993
- [5] H. Poincaré, *Les Méthodes Nouvelles de la Mécanique Céleste*, Gauthier-Villars, Paris, 1892, Vol.3, pg. 382
- [6] H. Poincaré, *Les Méthodes Nouvelles de la Mécanique Céleste*, Gauthier-Villars, Paris, 1892, Vol.3, pg. 397
- [7] J. Meiss, *Visual explorations of dynamics: the standard map*, Pramana - Journal of Physics 1-23 (2008)
- [8] T.L. Vincent. & Mees, *Controlling a Bouncing Ball*, International Journal of Bifurcation and Chaos 10, 579-592 (2000)
- [9] T.L. Vincent, *Chaotic Control Systems*, Nonlinear Dynamics and Systems Theory 1, 205-218 (2001)
- [10] J. Ghosh, *Control of 2-periodic motion for bouncing ball*, Control Conference, 1999, Proceedings 4048-4050 (1999)